PLANT SCIENCES

Differential phosphorylation of receptor kinase SlLYK4 mediates immune responses to bacterial and fungal pathogens in tomato

Wanting Zhu[1,2,3]†, Sen Cao[1,2,3]†, Mengling Huang[1,2,3], Pengyue Li[1,2,3], Jingjing Ke[1,2,3], Ai Xu[1,2,3], Yang Lin[3], Jiatao Xie[1,2,3], Jiasen Cheng[1,3], Yanping Fu[3], Daohong Jiang[1,2,3], Xiao Yu[1,2,3], Bo Li[1,2,3]*

Bacterial wilt caused by *Ralstonia solanacearum* is a devastating plant disease. Exopolysaccharide (EPS), a major virulence factor of *R. solanacearum*, elicits pattern-triggered immunity (PTI) in tomato, but the means by which EPS is recognized in the plant remain poorly understood. We found that tomato non-arginine-aspartate (non-RD) receptor kinase SlLYK4 mediates the perception of *R. solanacearum* EPS and positively regulates resistance to bacterial wilt. The RD receptor kinases SlLYK1 and SlLYK13 are required for EPS-triggered immune responses and form complexes with SlLYK4. These receptor kinase complexes have dual functions in recognizing bacterial EPS and fungal chitin. Phosphorylation of serine-320 in the juxtamembrane domain of SlLYK4 is essential in EPS- and chitin-mediated signaling, whereas phosphorylation of serine-334 or serine-634 in the C-terminal domain is required for chitin or EPS signaling, respectively. Our results reveal the mechanism underlying EPS recognition in tomato and provide insight into how differential phosphorylation of receptor kinase regulates antibacterial and antifungal immunity.

INTRODUCTION

Plants rely on a robust immune system to defend against potentially harmful microbes in the surrounding environment. Plant cell surface–localized pattern recognition receptors (PRRs) detect microbe-associated molecular patterns (MAMPs) of various pathogens or damage-associated molecular patterns derived from plant tissues (*1*). Plant PRRs include receptor-like proteins (RLPs) and receptor-like kinases (RLKs), which are classified by whether the intercellular domain contains a kinase domain (KD) (*2*). A typical plant RLK contains an ectodomain, a transmembrane domain, a juxtamembrane (JM) domain, and a cytoplasmic KD (*3*). The ectodomains of PRRs located outside the cell membrane are multivariant, such as the leucine-rich repeat (LRR) domain, lysine motif (LysM), and lectin domain, which provide the means to recognize a diversity of ligands. For example, the LRR-type PRRs FLAGELLIN SENSING 2 (FLS2) in *Arabidopsis* and FLS3 in tomato detect epitope peptides from bacterial flagellin, whereas *Arabidopsis* lysin motif receptor kinase 5 (AtLYK5) and the rice chitin elicitor binding protein (OsCEBiP) perceive fungal cell wall–derived chitin oligomers (*4*, *5*). Similarly, tomato LysM receptor kinase 4 (SlLYK4) and SlLYK1, which is named as chitin elicitor receptor kinase 1 (SlCERK1), have been found to play roles in mediating chitin signaling (*6*). It has been well recognized that LysM-type PRRs are mainly involved in the binding of carbohydrate MAMPs (*7*).

Once PRRs perceive the corresponding ligand, intermolecular conformation changes occur and the receptor complex initiates pattern-triggered immunity (PTI) (*8*). Co-receptors, including somatic embryogenesis receptor kinase (SERK) family members for the LRR-type PRRs or chitin elicitor receptor kinase 1 (CERK1) for LysM-type PRRs, are recruited into the complex in addition to receptor-like cytoplasmic kinases (RLCKs) (*7*, *9*). A series of phosphorylation events between the receptor and co-receptor cytoplasmic domains (CDs) to activate immune signaling after ligands is perceived. Most RLKs are Arg-Asp (RD) kinases with Arg in the catalytic loop HRD motif, which catalytic activity depends on the phosphorylation of the activation loop. Compared to RD kinases, the catalytic and autophosphorylation activities of non-arginine-aspartate (non-RD) kinases are low and the phosphorylation of the activation loop is not required for their function (*10*). MtLYR4, a member of LYR subfamily in *Medicago truncatula*, has both auto- and transphosphorylation activity in vitro (*11*). Subsequently, the signal from the cell membrane surface is quickly transmitted intracellularly, which enables the rapid activation of defensive response (*12*). Typical PTI events include calcium influx, extracellular alkalization, production of reactive oxygen species (ROS), activation of mitogen-activated protein kinase (MAPK) cascades, deposition of callose, and transcriptional reprogramming (*7*). The broad-spectrum, limiting effect of PTI can protect plants against a variety of pathogens.

Bacterial wilt caused by *Ralstonia solanacearum* occurs in a notably broad range of plants and is a devastating plant disease (*13*). Many major virulence factors assist *R. solanacearum*, such as type II–secreted plant cell wall–degrading enzymes, exopolysaccharide (EPS), swimming motility, and biofilms (*14*, *15*). In addition, type III effectors function inside host plant cells, which suppress plant defense mechanisms and modulate host metabolism (*16*). As a major virulence factor of *R. solanacearum*, EPS contributes to occlusion of the xylem vessels and eventually causes characteristic plant wilting symptoms (*15*). Unfortunately, *Ralstonia* resistance and immune mechanisms in tomatoes are poorly characterized. Tomato plants cannot recognize flg22 and elf18 from *Ralstonia* (two common bacterial MAMPs) and induce PTI (*17*, *18*). Bacterial cold shock protein does trigger an immune response in Solanaceae species and the receptor COLD SHOCK PROTEIN RECEPTOR

[1]National Key Laboratory of Agricultural Microbiology, Huazhong Agricultural University, Wuhan, Hubei 430070, China. [2]Hubei Hongshan Laboratory, Wuhan, Hubei 430070, China. [3]The Provincial Key Lab of Plant Pathology of Hubei Province, College of Plant Science and Technology, Huazhong Agricultural University, Wuhan, Hubei 430070, China.
*Corresponding author. Email: boli@mail.hzau.edu.cn
†These authors contributed equally to this work.

(SlCORE) in tomato has been identified (*19*, *20*). Recently, we found exo-PG PehC is a specific immune elicitor from *Ralstonia*; however, the cognate receptor remains to be identified (*21*). Our understanding of how tomato plants perceive the bacterial wilt pathogen requires further research.

Bacterial EPS, a highly polymerized, hydrated, anionic pericellular matrix, can protect the bacterial cell from negative environmental factors and host plant defenses (*22*). The wild-type strain GMI1000 of *R. solanacearum* produces three types of EPSs, including a high–molecular weight acidic polymer (EPS 1) that accounts for up to 90% of the dry weight of EPSs and two minor polymers, an *N*-acetylglucosaminorhamnan (EPS 3) and a glucan (EPS 4) (*23*). The EPS 1 synthesis mutant strains were hypoaggressive and rarely caused wilt symptoms compared to the wild-type strain (*22*, *24*). However, instead of functioning as a virulence factor, EPS can also function as an immune elicitor in plants. Purified EPS has been shown to activate the expression of the salicylic acid (SA) pathway defense gene GluA and initiate ROS accumulation in the resistant tomato variety Hawaii 7996, indicating that *R. solanacearum* EPS is an immune elicitor in tomato (*25*). Eggplant seedlings pretreated with *R. solanacearum* EPS also showed a notable increase in seed germination and growth, as well as a decreased incidence of bacterial wilt disease under greenhouse conditions (*26*). Nevertheless, there has been little progress in understanding EPS recognition by tomato.

In this study, we identified the tomato LysM-type PRR SlLYK4 for *R. solanacearum* EPS perception and the activation of immune signaling. SlLYK4 can form a complex with SlLYK1 and SlLYK13 that mediates immune responses triggered by EPS and chitin. Mutations in *SlLYK4*, *SlLYK1*, or *SlLYK13* compromise tomato resistance to bacterial wilt and Fusarium wilt disease. As a non-RD kinase, the kinase activity of SlLYK4 is essential for signal activation, which can enhance the phosphorylation of the RD kinases SlLYK13 and SlLYK1. Ser^{320} of SlLYK4 plays a crucial biological role in both EPS and chitin signaling pathways, whereas Ser^{334} exclusively contributes to chitin signaling. Furthermore, the Ser^{634} residue located at the C terminus of SlLYK4 is critical for SlLYK4 function in EPS- but not chitin-induced immunity. Consequently, our research elucidated the mechanism by which the same tomato receptor kinase mediates immunity upon recognizing different pathogens.

RESULTS

SlLYK4 is essential for EPS recognition by tomato

To determine how tomato plants recognize *R. solanacearum* EPS and induce PTI, we purified EPS from GMI1000 liquid culture and tested the immunogenic activity in tomato roots. An ROS burst was detected in root sections after EPS application, in both the resistant Hawaii 7996 variety and the susceptible Moneymaker variety (Fig. 1A). EPS treatment induced MAPK activation and rapid ethylene production in the root tissues of Hawaii 7996, which are hallmarks of PTI (fig. S1, A and B). EPS induced a strong ROS burst in the leaves of Hawaii 7996, but in Moneymaker leaves, the induction was markedly diminished (fig. S1C). These results indicated that a receptor in cultivated tomatoes recognized *Ralstonia* EPS and activated an immune response. The corresponding receptor was likely expressed in both the roots and leaves of the resistant and susceptible variety but appeared to have reduced expression in leaves of susceptible variety.

Given that carbohydrate-related MAMPs are generally recognized by LysM-type PRRs in plants, we screened for the potential LYK receptor for *Ralstonia* EPS in tomato. The tomato genome encodes 13 lysin motif RLKs (*SlLYKs*), which can be grouped into two branches (*27*). One branch includes *SlLYK2/SlLYK4/SlLYK6-9*, which are non-RD kinases with an uncharged residue that precedes the conserved catalytic aspartate (D) residue in the KD. The remaining members are RD kinases that carry a positively charged arginine (R) adjacent to the D residue (fig. S1D). According to previous studies, LysM-PRRs (as ligand perceiving receptors) are usually non-RD kinases and form complexes with an RD kinase that acts as a co-receptor. Thus, we first silenced the *SlLYKs* from the non-RD kinase branch in Hawaii 7996 leaves by virus-induced gene silencing (VIGS) to test the recognition of EPS. Reverse transcription quantitative polymerase chain reaction (RT-qPCR) analysis was used to confirm the silencing of *SlLYKs* in Hawaii 7996 leaves (fig. S1E). We found that EPS-induced ROS production decreased significantly in *SlLYK4*-silenced tomato leaves; however, silencing other *SlLYKs* only slightly affected ROS production (Fig. 1B). These data suggested that SlLYK4 is involved in perception of EPS in tomatoes.

To verify the function of SlLYK4 in the recognition of *R. solanacearum* EPS, we generated a *SlLYK4* knockout mutant by CRISPR-Cas9 genome editing in resistant and susceptible cultivars. The homozygous mutant *sllyk4-H1* in the Hawaii 7996 background contained an adenine insertion that caused a frameshift mutation leading to a premature stop codon (Fig. 1C). In the Moneymaker background, *sllyk4-M8* was generated with a 23–base pair (bp) deletion that led to the early termination of protein translation (Fig. 1C). These *sllyk4* mutants exhibited similar plant height and root length compared to wild-type plants, suggesting that SlLYK4 is not involved in normal plant growth and development (fig. S2, A to C). Notably, both the *sllyk4-H1* and *sllyk4-M8* mutants almost completely lost the EPS-induced ROS burst in the roots (Fig. 1D) and EPS-induced ROS production decreased significantly in *sllyk4-H1* leaves (fig. S3A). Meanwhile, expression of the immune genes *SlERF2a*, *SlERF2b*, and *SlWRKY3* and the accumulation of callose upon EPS treatment were substantially blocked in the *sllyk4* mutants relative to the wild type (Fig. 1, E to G). MAPK activation triggered by EPS was also abolished in the *sllyk4-M8* mutant roots (fig. S3B). The above data indicated that SlLYK4 plays a critical role in bacterial EPS perception in tomato plants.

Because SlLYK4 is an ortholog of *Arabidopsis* chitin receptor AtLYK4 and AtLYK5, and a recent study showed that SlLYK4 could perceive chitin in tomato (*6*) (fig. S1D), we confirmed the function of SlLYK4 in chitin signaling in tomato. A notable reduction in MAPK phosphorylation was observed in *sllyk4* mutants upon chitin elicitation (fig. S3, C and D). Chitin treatment induced ROS production in root tissues of the wild type but not in those of *sllyk4-H1* and *sllyk4-M8* mutants (fig. S3, E and F). To investigate whether SlLYK4 participates in other PTI pathways, we examined the flg22-triggered immune response in *sllyk4* mutants. The *sllyk4-H1* and *sllyk4-M8* mutants demonstrated similar ROS production relative to corresponding wild-type plants after flg22 treatment (fig. S3, G and H), suggesting that SlLYK4 specifically functions in carbohydrate-based PAMP signaling. In addition, we tested SlLYK4 expression level in leaves/roots of Hawaii 7996 and Moneymaker. The expression level of SlLYK4 is comparable in leaves and roots in the resistant variety Hawaii 7996; however, their expression in leaves is significantly lower than that of roots in the susceptible variety moneymaker leaves, which could further explain why the EPS-triggered immunity is relatively weak in the leaves of susceptible variety (fig. S3I). Collectively, these results indicate that SlLYK4 is the indispensable signaling

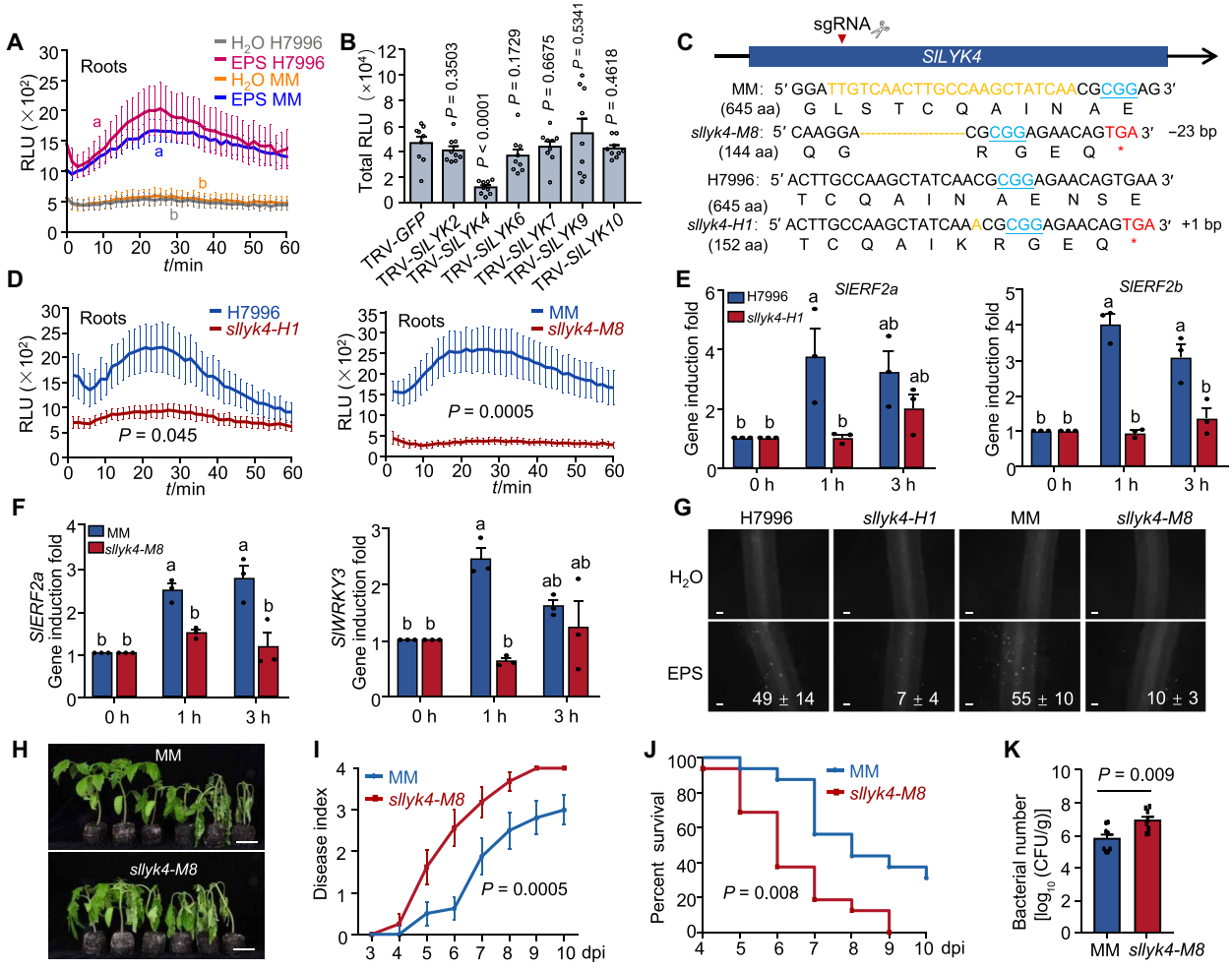

Fig. 1. SlLYK4 is required for EPS-induced immunity and resistance to *R. solanacearum*. (**A**) EPS-induced ROS burst in Hawaii 7996 (H7996) and Moneymaker (MM) roots. Values represent the means ± SE ($n = 10$). RLU, relative light units. (**B**) EPS-triggered ROS burst in tomato leaves silencing *SlLYKs* encoding non-RD kinases in H7996. Values represent the means ± SE ($n \geq 8$). (**C**) CRISPR-Cas9–mediated knockout of *SlLYK4* in MM and H7996. aa, amino acids. (**D**) EPS-induced ROS burst in wild-type (WT) and *sllyk4* mutant roots. Values represent the means ± SE ($n = 10$). (**E**) EPS-induced *SlERF2a* and *SlERF2b* expression in roots. Values represent the means ± SE ($n = 3$ technical replicates from one biological experiment). h, hours. (**F**) EPS-induced *SlERF2a* and *SlWRKY3* expression in roots of MM and *sllyk4-M8*. (**G**) EPS-induced callose deposition in WT and *sllyk4* mutant roots. Values at the bottom represent means ± SE from 10 photos of five individual plants. Scale bars, 50 μm. (**H**) Disease phenotype of MM and *sllyk4-M8* upon GMI1000 infection. Pictures were taken at 7 dpi post-GMI1000 inoculation. Scale bars, 4 cm. (**I**) Disease index of MM and *sllyk4-M8* post-GMI1000 inoculation. Data points represent the average disease index ± SE ($n = 16$ individual plants in one biological experiment). (**J**) Survival ratio was analyzed by comparing the number of survival plants to total plants from the data in (I). The Kaplan-Meier estimates survival analysis was performed, and the *P* value was analyzed by the log-rank (Mantel-Cox) test. (**K**) Bacterial titers of *R. solanacearum* in MM and *sllyk4-M8* stems. Tomato stems were collected at 7 dpi. Error bars represent ± SE ($n = 11$ individual plants). Significance of difference in [(B), (D), (E), (F), and (K)] was examined by a *t* test, and the *P* value is labeled at the top of the image. Different letters in (A) represent significant differences by one-way ANOVA analysis ($P < 0.05$). The above experiments were repeated three times with similar results. dpi, days postinoculation.

component for *R. solanacearum* EPS, and SlLYK4 also plays an important role in chitin perception.

SlLYK4 contributes to resistance to bacterial and fungal pathogens

To investigate whether SlLYK4 is involved in tomato resistance to *R. solanacearum*, 4-week-old *sllyk4* mutants were infected with *R. solanacearum*. Upon infection with the virulent strain UW551, the *sllyk4-H1* resistance to *R. solanacearum* was similar to that of the wild-type Hawaii 7996 (fig. S3J). During 6 to 12 days postinoculation (dpi), the *sllyk4-H1* mutant had a similar disease index and survival rate to wild-type plants (fig. S3, K and L). Meanwhile, bacterial titers in both upper and lower parts of the stem were slightly increased in *sllyk4-H1* mutant relative to the Hawaii 7996 plants (fig. S3M). Consistently, the *sllyk4-M8* mutant was more susceptible than the wild-type Moneymaker to *R. solanacearum* GMI1000 strain infection (Fig. 1H) and had a much higher disease index (Fig. 1I), significantly lower survival rate (Fig. 1J), and higher population density in the stems (Fig. 1K). These results suggested that SlLYK4 contributes to tomato resistance toward *R. solanacearum*. Given the function of SlLYK4 in chitin signaling, we assessed the role of SlLYK4 in fungal pathogen resistance. A spore suspension of *Fusarium oxysporum* f. sp. *lycopersici* (race 2) (*Fol*) FGSC 9935 was inoculated into the *sllyk4-M8* mutant. We found that the *sllyk4-M8* mutant was

more susceptible to *Fol*, and the disease index was significantly higher than in the wild type (fig. S3, N to P), suggesting that SlLYK4 also positively regulates resistance to fungi in tomato.

To further investigate the function of SlLYK4 in resistance to *R. solanacearum*, SlLYK4 under the control of the 35*S* promoter was transiently overexpressed in roots of the susceptible variety Moneymaker by *Agrobacterium rhizogenes*–mediated hairy root transformation. The expression of SlLYK4 was confirmed by immunoblotting (fig. S4A). Significantly enhanced resistance to GMI1000 was observed in SlLYK4 overexpressing plants relative to control plants transformed with an empty vector (fig. S4B). In addition, the disease index was significantly lower and the survival rate was much higher in SlLYK4 overexpressing plants than in control plants (fig. S4, C and D). Furthermore, the stems of SlLYK4 overexpressing tomatoes accumulated less *R. solanacearum* relative to the control plants, indicating that overexpression of SlLYK4 limited the proliferation of *R. solanacearum* in the xylem (fig. S4E). We also generated stable SlLYK4 overexpression transgenic lines in the susceptible Alisa Craig background (fig. S4F). Enhanced resistance to GMI1000 was observed in the stable overexpression plants, as evidenced by a lower disease index and slower disease progression (fig. S4, G and H). Together, these results demonstrate that SlLYK4 plays a key role in resistance to *R. solanacearum*.

SlLYK1 and SlLYK13 positively regulate EPS-triggered responses

Because SlLYK4 is a non-RD protein kinase, we speculated that another SlLYK (in the branch of RD-LYKs) serves as a co-receptor for SlLYK4 and participates in EPS recognition. To test our conjecture, we individually silenced the RD-type *SlLYKs* in Hawaii 7996 leaves by VIGS (fig. S5A). The EPS-induced ROS burst was largely compromised in the leaves of *SlLYK1*- and *SlLYK13*-silenced tomato plants compared with that in the control plants (Fig. 2A). To further explore the involvement of SlLYK1 and SlLYK13 in EPS perception, we generated the *SlLYK1* mutant line by CRISPR-Cas9 technology in the Moneymaker background (Fig. 2B) and no difference in plant height and root length was observed between these *sllyk1* mutants and wild-type tomatoes (fig. S5, B to D). A homozygous mutant *sllyk1-M17* was obtained with a nucleotide insertion in the first exon of *SlLYK1*, which caused an early termination of translation (Fig. 2B). The EPS-induced ROS burst and MAPK activation were completely abolished in the roots of *sllyk1-M17* mutants (Fig. 2, C and D). Two immune marker genes, *SlWRKY3* and *SlERF2b*, showed elevated expression in the roots upon EPS treatment in the wild-type background but not in *sllyk1* mutants (Fig. 2E). In addition, EPS-induced callose deposition was compromised in *sllyk1-M17* roots compared with that in roots of the wild type (Fig. 2F). These data suggested that SlLYK1 is required for EPS-induced immunity in tomato roots.

Next, we tested SlLYK13 function in EPS-mediated immune responses. The homozygous mutant *sllyk13-M4* was obtained by CRISPR-Cas9 to target the DNA sequence in the first LysM domain of *SlLYK13* in the Moneymaker background (Fig. 2G). The *sllyk13-M4* mutant has a five-nucleotide deletion, which leads to the early termination of protein translation (Fig. 2G). The plant height and root length of *sllyk13-M4* mutants are similar with the wild-type plant (fig. S5, B to D). Then, we examined EPS-induced PTI responses in the *sllyk13-M4* mutant. Upon EPS treatment, the ROS burst and MAPK phosphorylation were totally blocked in the roots of the *sllyk13-M4* mutant (Fig. 2, H and I). Expression of *SlWRKY3* and *SlERF2b* could not be induced by EPS in *sllyk13* mutants (Fig. 2J). In addition, EPS-triggered callose accumulation in the *sllyk13-M4* mutant was notably lower than in the wild type (Fig. 2K). These results suggested that SlLYK13 plays a critical role in EPS-induced immunity in tomatoes.

Because SlLYK4 and SlLYK1 have been reported to be required for chitin responses in tomato (*6*), we tested whether chitin-induced PTI responses were impaired in *sllyk1* and *sllyk13* mutants. The chitin-induced ROS burst was almost completely blocked in the *sllyk1* mutant, and a 50% reduction in ROS production occurred in the *sllyk13* mutant, compared to the wild type (Fig. 2L). In addition, a significant reduction in chitin-triggered MAPK phosphorylation was observed in the roots of the *sllyk13* mutant (fig. S5E). Thus, both SlLYK1 and SlLYK13 contribute to chitin responses, although SlLYK1 contributes more than SlLYK13. The production of ROS in *sllyk13-M4* roots was comparable to that in wild-type roots upon flg22 treatment, suggesting that SlLYK13 does not participate in flg22-induced immune signaling (fig. S5F).

SlLYK1 and SlLYK13 positively regulate tomato resistance to *R. solanacearum*

Given that both SlLYK1 and SlLYK13 are indispensable for EPS-triggered immunity in tomato, we evaluated their contribution to bacterial wilt resistance. Moneymaker and *sllyk1* mutant plants were challenged with GMI1000 by soil soaking inoculation. The mutant plants experienced faster disease progress and wilt symptoms than the wild-type plants (Fig. 3A). The disease index was significantly higher, and the survival rate was lower, in the *sllyk1* mutant plants than in the Moneymaker plants (Fig. 3, B and C). Bacterial multiplication was ~10 times greater in *sllyk1* mutant stems than in wild-type stems at 5 dpi (Fig. 3D). Furthermore, we transiently overexpressed 35*S* promoter–driven SlLYK1 with a C-terminal hemagglutinin (HA) epitope tag in Moneymaker plants by hairy root transformation (fig. S5G). Expectedly, the overexpression of SlLYK1 significantly enhanced tomato resistance to *R. solanacearum* (Fig. 3E); these plants had a higher disease index and lower survival rate than the wild-type plants (Fig. 3, F and G). We quantified *R. solanacearum* in the stems of SlLYK1 overexpression plants, and the bacterial titers showed a significant decrease relative to the wild type (Fig. 3H). Thus, SlLYK1 positively contributes to *R. solanacearum* resistance in tomatoes.

Next, we tested whether SlLYK13 regulates tomato resistance to *R. solanacearum*. The *sllyk13-M4* mutant showed more serious wilt symptoms upon GMI1000 infection compared to the wild-type Moneymaker (Fig. 3I), as well as a higher disease index and lower survival rate than wild-type plants at 4 to 12 dpi (Fig. 3, J and K). After 5 dpi, *sllyk13-M4* plants had a significantly higher density of *R. solanacearum* in the stems (Fig. 3L). In Moneymaker plants, SlLYK13 with a C-terminal HA epitope tag driven by the 35*S* promoter was transiently overexpressed via tomato hairy root transformation (fig. S5H). Expectedly, the overexpression of SlLYK13 significantly enhanced tomato resistance to *R. solanacearum* (Fig. 3M); these plants had a higher disease index and lower survival rate than the wild-type plants (Fig. 3, N and O). We further quantified *R. solanacearum* in the stems of the tomato plants. The bacterial titers in SlLYK13 overexpression plants decreased significantly relative to the wild type (Fig. 3P). In summary, these results suggested that both SlLYK13 and SlLYK1 were both involved in tomato resistance to *R. solanacearum*.

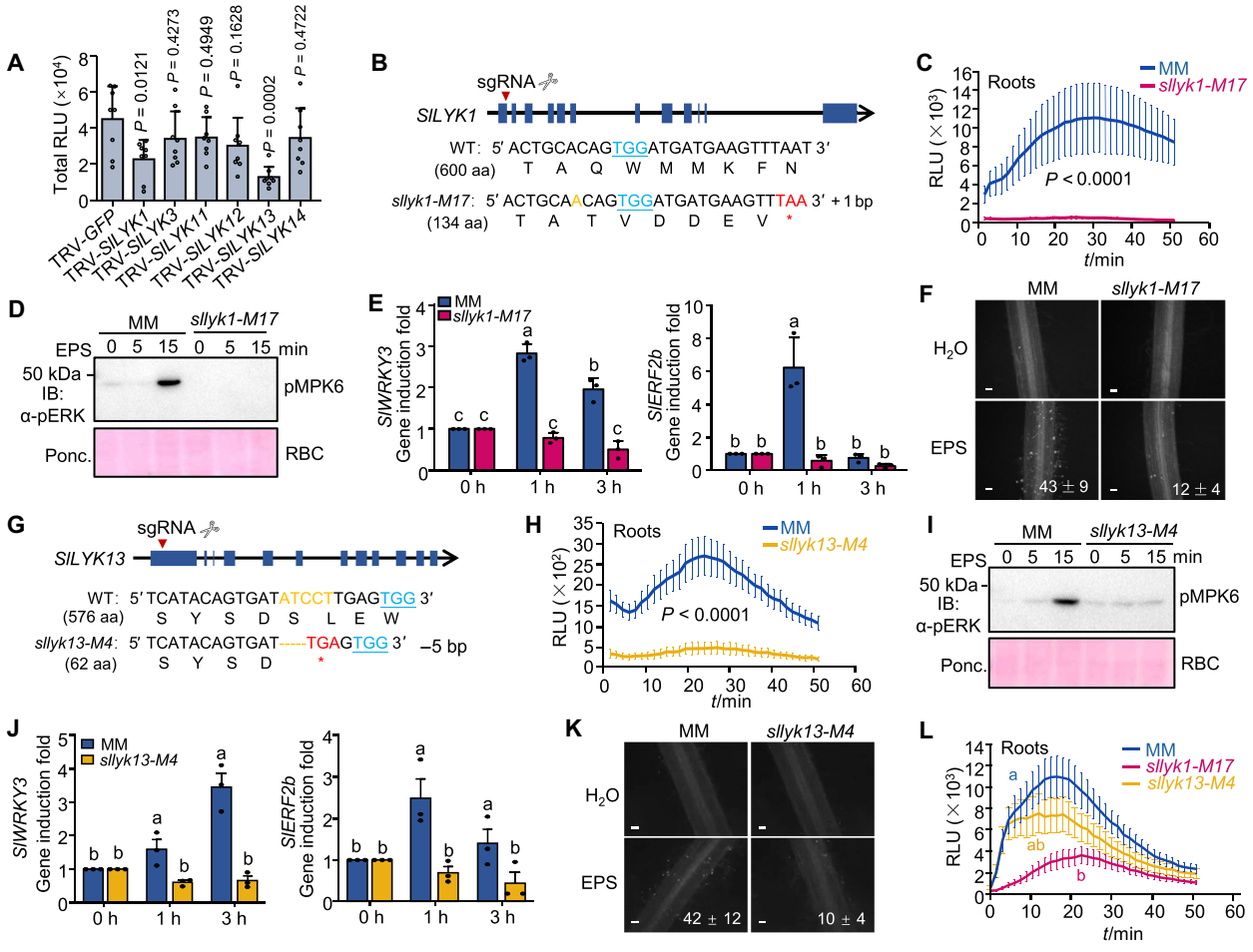

Fig. 2. SlLYK1 and SlLYK13 are required for EPS-induced immune responses. (**A**) EPS-induced ROS burst in Hawaii 7996 leaves silencing *SlLYKs* encoding RD kinases. Values represent the means ± SE ($n = 8$). (**B**) CRISPR-Cas9–mediated knockout of *SlLYK1* in the MM background. The PAM sequences are shown in blue with an underline. (**C**) EPS-activated ROS burst in WT and *sllyk1-M17* roots. Values represent the means ± SE ($n = 9$). (**D**) EPS-induced MAPK activation in WT and *sllyk1-M17* roots. MAPK activation was detected by immunoblotting (IB) using an α-pERK1/2 antibody (top), and protein loading was shown by Ponceau S (Ponc.) staining for RuBisCO (ribulose-1,5-bisphosphate carboxylase/oxygenase) (RBC; bottom). (**E**) EPS-induced *SlWRKY3* and *SlERF2b* expression in MM and *sllyk1-M17* roots. Values represent the means ± SE ($n = 3$ technical replicates from one biological experiment). (**F**) EPS-triggered callose deposition in WT and *sllyk1-M17* roots. Values at the bottom represent means ± SE from five individual plants. Scale bars, 50 μm. (**G**) CRISPR-Cas9–mediated knockout of *SlLYK13* in the MM background. (**H**) EPS-activated ROS burst in MM and *sllyk13-M4* roots. Values represent the means ± SE ($n = 10$ individual plants). (**I**) EPS-induced MAPK activation in MM and *sllyk13-M4* roots. (**J**) EPS-induced *SlWRKY3* and *SlERF2b* expression in MM and *sllyk13-M4*. Values represent the means ± SE ($n = 3$). (**K**) EPS-triggered callose deposition in WT and *sllyk13-M4*. Values represent means ± SE from five individual plants. Scale bars, 50 μm. (**L**) Chitin-activated ROS burst in MM, *sllyk1-M17*, and *sllyk13-M4*. Values represent the means ± SE ($n = 12$ individual plants). The significance of difference in [(A), (C), (E), (H), and (J)] was examined by Student's *t* test. Different letters in (L) represent significant differences by one-way ANOVA analysis ($P < 0.05$). The above experiments were repeated three times with similar results. h, hours.

SlLYK4 interacts with both SlLYK1 and SlLYK13

Because SlLYK4, SlLYK13, and SlLYK1 are all involved in EPS-triggered immunity, we monitored protein interactions both in vivo and in vitro. A coimmunoprecipitation (Co-IP) assay was performed by coexpression of FLAG-tagged and HA-tagged SlLYK4 in *Nicotiana benthamiana* leaves, which confirmed the self-association of SlLYK4 independent of EPS treatment (Fig. 4A). Notably, SlLYK4-FLAG coimmunoprecipitated SlLYK13-HA independent of EPS treatment in the Co-IP assay (Fig. 4B). After transient expression in *N. benthamiana*, we observed that SlLYK1 shows a rapid mobility shift upon EPS treatment (fig. S6A) and the mobility shift was reversed by phosphatase λPP treatment, indicating that the band shift was due to SlLYK1 phosphorylation. Moreover, SlLYK1-HA could be immunoprecipitated by SlLYK4, and the interaction between SlLYK1 and SlLYK4 was enhanced upon EPS treatment (Fig. 4C). To confirm their interaction in planta, we performed a bimolecular fluorescence complementation (BiFC) assay in *N. benthamiana* leaves. The self-association of SlLYK4 on the plasma membrane was shown by a plasma membrane–localized Venus signal (Fig. 4D). In addition, SlLYK4 associated with SlLYK13 in the BiFC assay (Fig. 4D). EPS treatment promoted the interaction between SlLYK1 and SlLYK4 in the BiFC assay, which was consistent with the result from the Co-IP assay. Furthermore, $SlLYK4^{km}$ interacts more strongly than SlLYK4 with SlLYK1 in the absence of EPS (Fig. 4E). These data demonstrate that SlLYK4 self-interacts and forms complexes with SlLYK13 and SlLYK1.

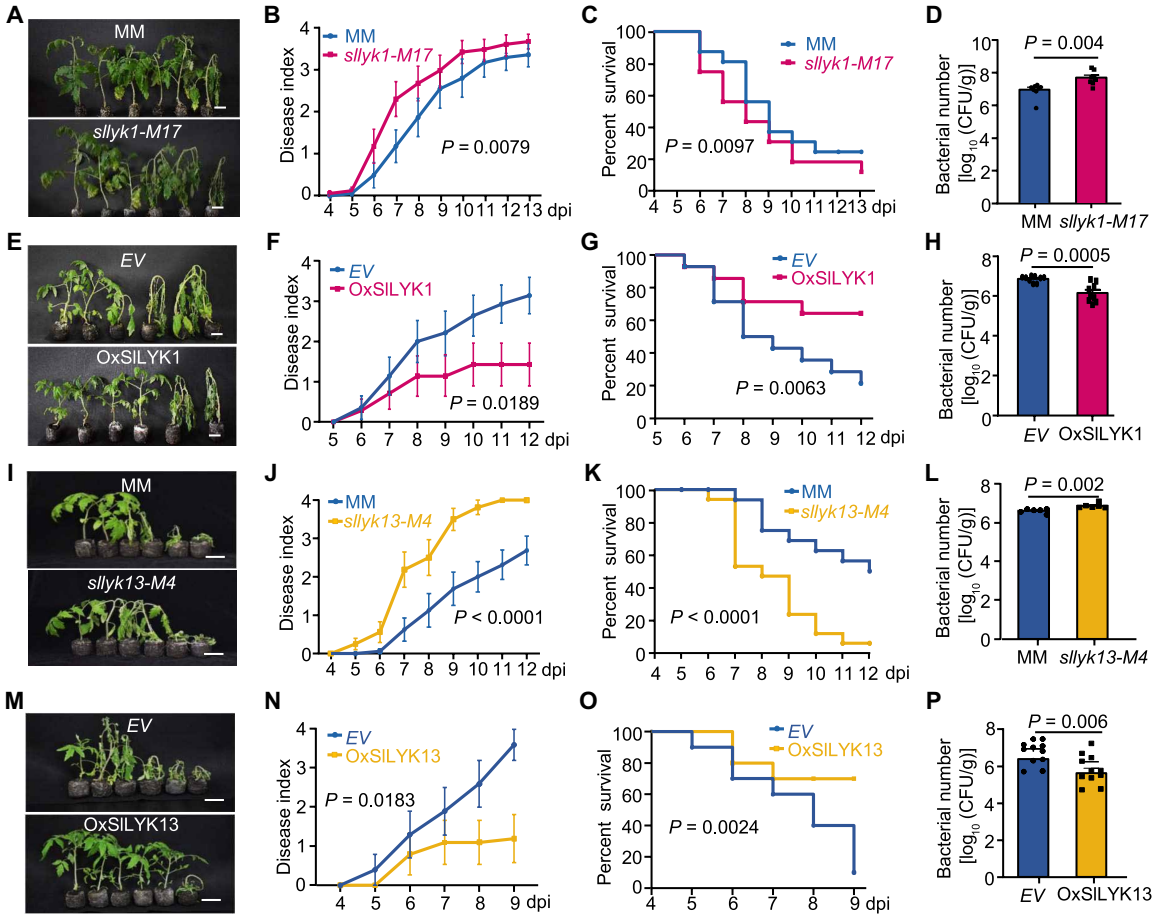

Fig. 3. SlLYK1 and SlLYK13 contribute to tomato resistance to *R. solanacearum*. (**A** to **D**) *sllyk1-M17* shows compromised resistance to GMI1000. Data points in disease index (B) represent means ± SE ($n = 16$ individual plants). The survival ratio (C) was analyzed by comparing the number of survival plants to the total plants from the data in (B). Bacterial growth number of tomato stems (D) was quantified at 5 dpi and shown as means ± SE ($n = 8$ stem sections). (**E** to **H**) Overexpression of *SlLYK1* enhances tomato resistance to GMI1000. Data points in disease index (F) represent means ± SE ($n = 10$). Bacterial growth (H) was quantified at 8 dpi and shown as means ± SE ($n = 9$). (**I** to **L**) *sllyk13-M4* shows compromised resistance to GMI1000. Data points in disease index (J) represent means ± SE ($n = 16$). Bacterial growth (L) was quantified at 5 dpi and shown as means ± SE ($n = 6$ individual plants). (**M** to **P**) Overexpression of *SlLYK13* enhances tomato resistance to GMI1000. Data points in disease index (N) represent means ± SE ($n = 10$). Bacterial growth (P) was quantified at 8 dpi and shown as means ± SE ($n = 12$). Symptom pictures in [(A), (E), (I), and (M)] were taken at 8 dpi. Scale bars in [(A), (E), (I), and (M)], 3 cm. In [(B), (F), (J), and (N)], the *P* value was analyzed by a LMM analysis. In [(G), (K), and (O)], the survival ratio was analyzed similarly as in (C). In [(C), (G), (K), and (O)], the *P* value was analyzed by the log-rank (Mantel-Cox) test. In [(D), (H), (L), and (P)], the significance of difference was examined by a *t* test. The above experiments were repeated three times with similar results.

Given that these are all membrane-localized RLKs, we further examined the direct interactions between their CDs, which encompass both the JM domain and the KD, in SlLYK4, SlLYK1, and SlLYK13. In the yeast two-hybrid assay, the KD of SlLYK4 (SlLYK4KD) interacted with the SlLYK13 KD (Fig. 4F). GST-SlLYK4CD, MBP-SlLYK1CD, and MBP-SlLYK13CD fusion proteins were expressed and purified from *Escherichia coli* using glutathione and dextrin beads. An in vitro pull-down assay indicated that glutathione Sepharose beads coupled with GST-SlLYK4CD directly pulled down MBP-SlLYK13CD-HA protein (Fig. 4G) and MBP-SlLYK1CD-HA protein (Fig. 4H). Together, the results demonstrated that SlLYK4 interacts directly with SlLYK13 and SlLYK1 through the CD.

The kinase activity of LYK4 is critical for its biological function

During transient expression in *N. benthamiana*, we found that coexpression of SlLYK4 and SlLYK13 induced a cell death–like phenotype. SlLYK13 but not SlLYK4 triggered weak cell death; however, coexpression of SlLYK4 and SlLYK13 triggered strong cell death in tobacco leaves at 3 dpi (Fig. 5A and fig. S6B). These results suggested that SlLYK4 and SlLYK13 were involved in the same biological process. We then generated kinase inactive mutants of SlLYK4 and SlLYK13, $SlLYK4^{km}$ (K380E) and $LYK13^{km}$ (K328E), by mutating lysine (K) to glutamate (E) in the conserved adenosine triphosphate (ATP)–binding site, and $SlLYK4^{D471N}$ (the HKD motif in catalytic loop was mutated to HKN). Coexpression of SlLYK13 with either $SlLYK4^{km}$ or $SlLYK4^{D471N}$ could not enhance the cell death induced by SlLYK13 (Fig. 5A). In addition, SlLYK4 and $SlLYK13^{km}$ coexpressed abolished cell death (Fig. 5A), suggesting that kinase activity of SlLYK4 and SlLYK13 is crucial for their biological function, regardless of whether they are a non-RD or an RD kinase. The electrolyte leakage results were in line with the cell death phenotype and showed that coexpression of SlLYK4 and SlLYK13 markedly increased ion leakage; however, $SlLYK4^{km}$ or $SlLYK4^{D471N}$ only slightly enhances SlLYK13-triggered

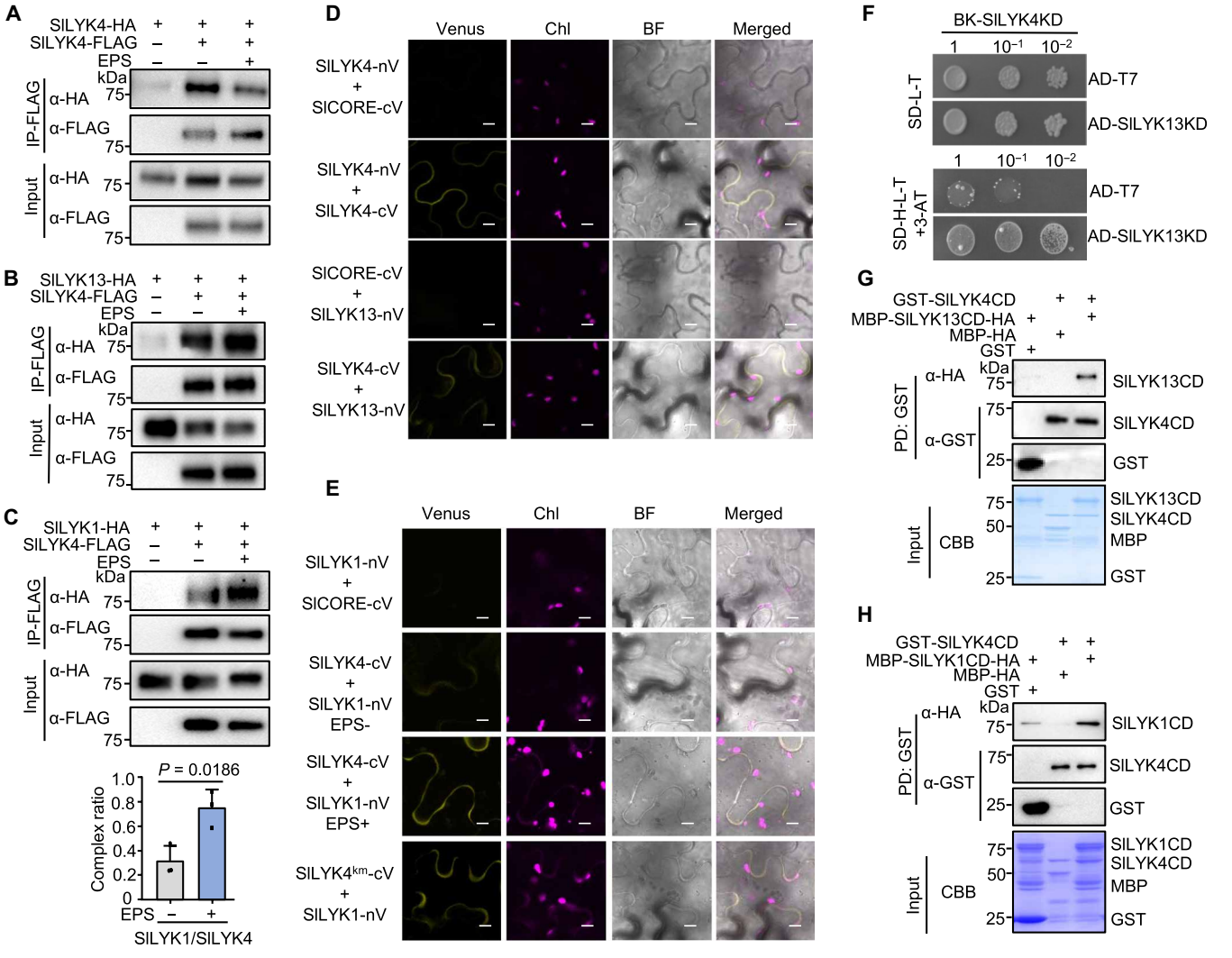

Fig. 4. Interaction and receptor complex formation of SlLYK4, SlLYK1, and SlLYK13. (**A**) Self-association of SlLYK4 in *N. benthamiana* leaves by Co-IP assay. (**B**) SlLYK4 associates with SlLYK13 in *N. benthamiana* leaves by Co-IP assay. (**C**) SlLYK4 associates with SlLYK1 in *N. benthamiana* leaves by Co-IP assay. EPS was infiltrated into *N. benthamiana* leaves that expressing HA-tagged and FLAG-tagged proteins. The complex was purified by immunoprecipitation with α-FLAG Agarose (IP: a-FLAG) and subjected to immunoblot analysis. Signal intensity was quantified using the ImageJ software; values represent the means ± SD ($n = 3$, three independent repeat signal ratio data), and the significance of difference was examined by a *t* test. (**D**) SlLYK4 forms a homologous dimer and interacts with SlLYK13 in *N. benthamiana* leaves by BiFC analysis. Scale bars, 30 μm. (**E**) SlLYK4 interacts with SlLYK1 in *N. benthamiana* leaves by BiFC analysis. Scale bars, 30 μm. The nVenus (nV) fusion proteins (N-terminal 158 amino acids of Venus) and cVenus (cV) fusion proteins (C-terminal 82 amino acids of Venus) were transiently coexpressed in *N. benthamiana* leaves. SlCORE-cV was used as a control. Chl, chloroplasts; BF, bright field. (**F**) The KD of SlLYK4 (SlLYK4KD) interacts with SlLYK13KD in a yeast two-hybrid assay. The interaction between SlLYK4KD and SlLYK13KD was tested on synthetic defined medium (SD-L-T-H) supplemented with 1 mM 3-AT. pGADT7 (AD) is the empty vector. (**G**) The CDs of SlLYK4 and SlLYK13 interact in an in vitro pull-down (PD) assay. GST or GST-SlLYK4CD immobilized on glutathione Sepharose beads was incubated with MBP or MBP-SlLYK13CD-HA proteins. (**H**) SlLYK4CD directly interacts with SlLYK1CD in vitro by PD assay. MBP and MBP-SlLYK1CD were incubated with GST-SlLYK4CD and pulled down with GST. Experiments were repeated three times independently with similar results.

ion leakage (Fig. 5B). Similarly, SlLYK1 alone could induce cell death in *N. benthamiana* leaves, but this phenotype was enhanced after coexpression with SlLYK4 (fig. S6, B and C). We also showed that SlLYK4^{km} could not enhance cell death induced by SlLYK1, demonstrating the important role of SlLYK4 kinase activity. Collectively, the kinase activity of non-RD kinase SlLYK4 is essential for its function.

Given that SlLYK4 and SlLYK13 form a complex and the kinase activity is essential their function, we conducted in vitro kinase assays to investigate the phosphorylation events of SlLYK4 and SlLYK13. Although SlLYK4 is a non-RD kinase, its CD (SlLYK4CD) exhibited clear autophosphorylation activity upon the addition of ATP-γ-S. In contrast, both the D471N variant and SlLYK4CD^{km} variant abolished kinase activity (Fig. 5C). The autophosphorylation level of SlLYK4CD and SlLYK4CD^{km} variant was also confirmed by immunoblotting with an anti-phospho-Thr/Tyr antibody (fig. S6E). Furthermore, an in vitro kinase assay using MBP-SlLYK4CD as a kinase and GST-SlLYK4CD^{km} as a substrate demonstrated that MBP-SlLYK4CD could phosphorylate GST-SlLYK4CD^{km}, indicating that SlLYK4 has trans-autophosphorylation activity (fig. S6F). In addition, we assessed the kinase activity of SlLYK4CD^{km} and D471N

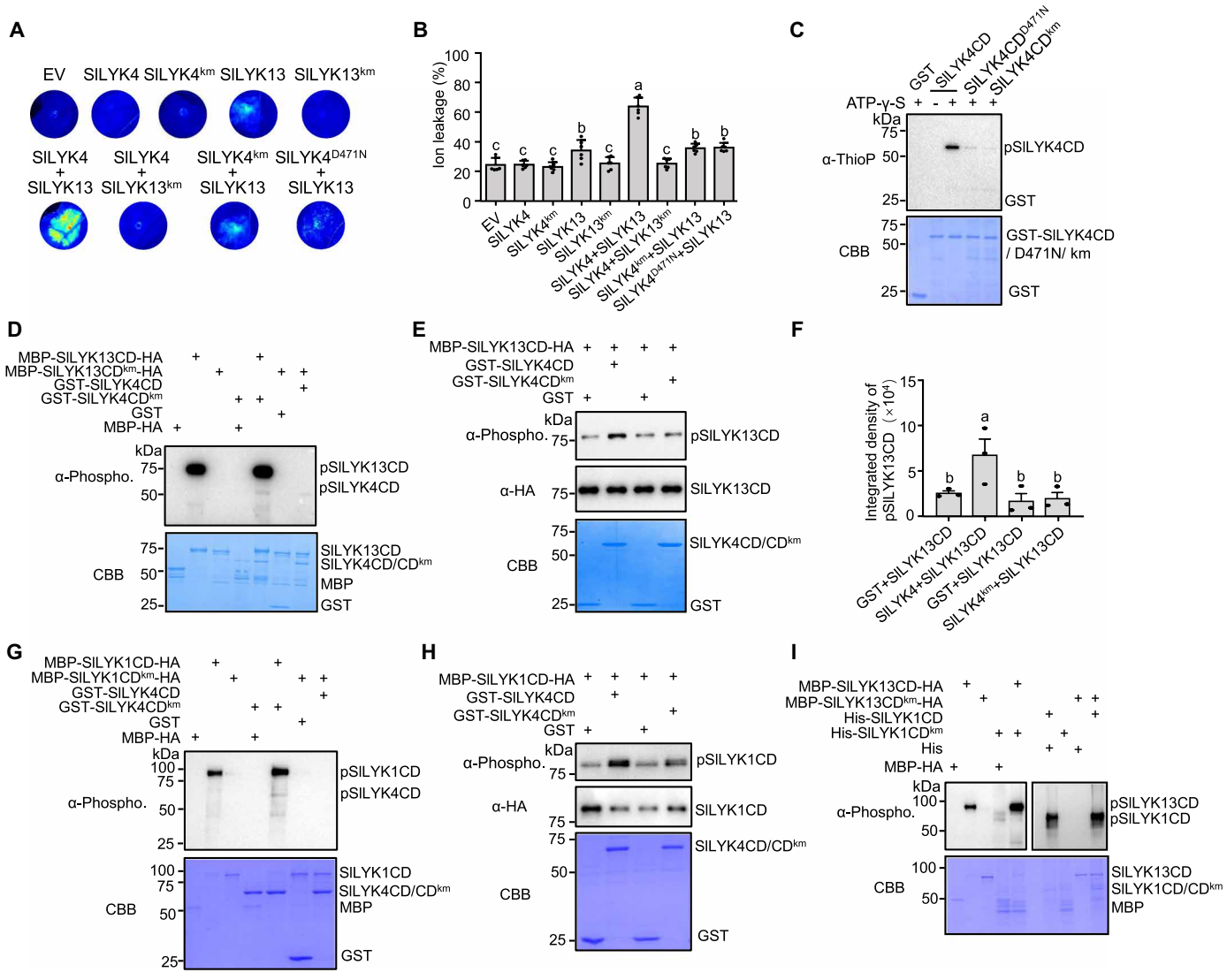

Fig. 5. The kinase activities of SlLYK4 and SlLYK13 are essential for their biological function. (**A**) Coexpression of SlLYK4 and SlLYK13, but not the kinase mutant (km) variants, induces cell death in *N. benthamiana* leaves. Combinations of *SlLYK13-HA*, *SlLYK13^{km}-HA*, *SlLYK4-FLAG*, *SlLYK4^{km}-FLAG*, or an *EV* were expressed in *N. benthamiana* leaves. Photographs were captured under ultraviolet light. (**B**) Cell death was quantified by measuring the electrolyte leakage. The agroinfiltrated leaves were collected at 72 hours, and their electrolyte leakage was measured with a conductivity meter. Values represent means ± SE ($n = 6$ leaves from different plants). (**C**) SlLYK4 undergoes autophosphorylation in vitro. The autophosphorylation of GST-SlLYK4CD and its km variant was analyzed by the anti-thiophosphate ester antibody (α-ThioP) (top) after incubation in protein kinase buffer containing ATP-γ-S and PNBM. Protein loading was shown by CBB (bottom). (**D**) SlLYK13 directly phosphorylates SlLYK4 in vitro. The autophosphorylation of MBP-SlLYK13CD and the phosphorylation relationship between MBP-SlLYK13CD and GST-SlLYK4CD were analyzed. (**E**) The kinase activity of SlLYK4 promotes the phosphorylation of SlLYK13. The kinase assay was performed by incubating GST-SlLYK4CD or GST-SlLYK4CD^{km} with MBP-SlLYK13CD, and the phosphorylation level of SlLYK13CD was detected. (**F**) Quantitative data for the signal intensity in (E) using the ImageJ software. Values represents means ± SE ($n = 3$, three independent repeat signal ratio data). (**G**) SlLYK1 phosphorylates SlLYK4 in vitro. The phosphorylation relationship between MBP-SlLYK1CD and GST-SlLYK4CD was detected. (**H**) The kinase activity of SlLYK4 promotes the phosphorylation of SlLYK1. The kinase assay was performed by incubating GST-SlLYK4CD or GST-SlLYK4CD^{km} with MBP-SlLYK1CD, and the phosphorylation level of SlLYK1CD was detected. (**I**) Detection of the phosphorylation relationship between MBP-SlLYK13CD and His-SlLYK1CD. Different letters in [(B) and (F)] indicate significant differences by one-way ANOVA analysis ($P < 0.05$). Experiments were repeated three times independently with similar results.

variants by monitoring ATP hydrolysis efficiency in kinase assays. The ATP hydrolysis reaction rate was significantly higher in the presence of SlLYK4CD compared to the negative control glutathione *S*-transferase (GST), whereas it remained relatively low for the km and D471N variants (fig. S6G). These results suggest that SlLYK4 exhibits both cis- or trans-autophosphorylation activities.

Likewise, SlLYK13CD displayed strong autophosphorylation activity detecting by immunoblotting with an anti-phospho-Thr/Tyr antibody, which was abolished in SlLYK13CD^{km} (Fig. 5D). An in vitro kinase assay using SlLYK13CD as the kinase and SlLYK4CD^{km} as the substrate indicated that SlLYK13CD could phosphorylate SlLYK4CD^{km} (Fig. 5D). However, we did not observe clear phosphorylation of SlLYK13CD^{km} by SlLYK4CD (Fig. 5D). When incubating SlLYK13CD with SlLYK4CD or SlLYK4CD^{km} in the kinase assay, SlLYK4CD, but not SlLYK4CD^{km}, stimulated SlLYK13CD phosphorylation more than threefold (Fig. 5, E and F). We also

tested phosphorylation between SlLYK4 and SlLYK1. SlLYK1CD showed autophosphorylation activity and was able to phosphorylate SlLYK4CD^{km} (Fig. 5G). Furthermore, GST-SlLYK4CD could stimulate MBP-SlLYK1CD phosphorylation (Fig. 5H). In addition, we performed an in vitro kinase assay to assess transphosphorylation between SlLYK1 and SlLYK13 and found that SlLYK13CD could not phosphorylate SlLYK1CD^{km} and that phosphorylation of SlLYK13CD^{km} by SlLYK1CD could not be detected (Fig. 5I). Overall, we demonstrated that SlLYK4, as a non-RD kinase, was able to enhance the phosphorylation of RD kinases SlLYK13 and SlLYK1, which may be an early step in immune signaling.

Phosphorylation of the JM and C-terminal domains is essential for SlLYK4 function

Kinase activity is vital for SlLYK4 function, so we attempted to identify the key phosphorylation residues of SlLYK4. First, we performed liquid chromatography–tandem mass spectrometry (LC-MS/MS) of GST-SlLYK4CD and MBP-SlLYK13CD or Maltose-Binding Protein (MBP) (mock) after in vitro kinase assays. We identified two phosphorylation sites Thr^{506} and Ser^{634} in SlLYK4 when incubation with MBP-SlLYK13CD but not with MBP (Fig. 6A, table S3, and data S1). Thr^{506}, which is a well-conserved residue in the catalytic loop of the KD, corresponds to the BAK1 Thr^{449} residue (*28*) and BIK1 Thr^{237} residue (*29*) and highly conserved in the LYRIIIA subfamily (fig. S7A). Another phosphorylation event occurred at Ser^{634} in the C-terminal domain, which is relatively conserved in the LYRIIIA subfamily (fig. S7B). Second, SlLYK4-FLAG was transiently expressed in tomato hairy roots and samples were collected post-EPS or chitin treatment, followed by immunoprecipitation and phosphorylation analysis by mass spectrometry (MS). At the resting stage, phosphorylation events were detected on Ser^{312} and Ser^{328} in the JM domain and Ser^{636}/Ser^{638}/Ser^{640} in the C-terminal domain of SlLYK4 (Fig. 6A, table S3, and data S1). Upon EPS elicitation, Ser^{320} in the JM domain and Ser^{634} in the C-terminal domain were identified as phosphorylation sites. Meanwhile, phosphorylation of Ser^{320} and Ser^{334} in the JM domain was observed following chitin treatment (Fig. 6A, table S3, and data S1). By aligning the JM domains of proteins in LYRIIIA subfamily, we found that all the in vivo phosphorylation residues were not conserved (fig. S7C).

To screen key phosphorylation residues for SlLYK4 function, the candidate threonine and serine sites were replaced by alanine to generate the phospho-dead variant. We tested the ability of the phospho-variants to induce cell death in *N. benthamiana* when coexpressed with SlLYK13 (fig. S8A). As expected, wild-type SlLYK4 strongly enhanced SlLYK13-induced cell death, and SlLYK4^{km} and SlLYK4^{T506A} almost block cell death. SlLYK4^{S320A}, SlLYK4^{S328A}, and SlLYK4^{S634A} could not promote the SlLYK13-induced cell death phenotype, whereas SlLYK4^{S334A} exhibited a slight enhancement (Fig. 6, B and C). Consistently, electrolyte leakage triggered by coexpression of SlLYK13 with these SlLYK4 variants was significantly compromised compared to that of the wild-type SlLYK4 (Fig. 6D). Because cell death induced by SlLYK1 can be enhanced after coexpression with SlLYK4, we investigated cell death activated by coexpression of SlLYK1 with these SlLYK4 variants in *N. benthamiana* leaves. The results showed that the above SlLYK4 variants largely abolished cell death with similar levels of expression (Fig. 6, E and F, and fig. S8B). Thus, these data indicated that phosphorylation of Ser^{320}/Ser^{328}/Ser^{334} in the JM domain and Ser^{634} in the C-terminal domain is required for LYK4 function.

To reveal whether these phosphorylation sites are required for SlLYK4 autophosphorylation and transphosphorylation to SlLYK13, we performed in vitro kinase activity assays with different variants. Strong autophosphorylation was detected in S328A and S334A mutants, but not in the S320A and S634A mutants, indicating that Ser^{320} and Ser^{634} are critical residues for the autophosphorylation of SlLYK4 (Fig. 6G). Then, SlLYK13CD phosphorylation enhancement by recombinant SlLYK4 or variant proteins was analyzed using ATP-γ-S as a phosphate donor in in vitro kinase assays. SlLYK13CD kinase activity was enhanced by the presence of SlLYK4CD but not SlLYK4CD^{km} or phosphosite mutants (Fig. 6H). These results suggest that the phosphorylation of Ser^{320}/Ser^{328}/Ser^{334} and Ser^{634} of SlLYK4 is important for phosphorylation with SlLYK13 in vitro. To further validate the function of the phosphorylation sites, the candidate sites were replaced by aspartic acid to generate the phosphomimetic variants and the cell death was monitored in *N. benthamiana* when coexpressed with SlLYK13 (fig. S8C). Cell death phenotype and electrolyte leakage triggered by coexpression of SlLYK13 with these phosphomimetic variants were similar to wild-type SlLYK4 (Fig. 6, I to K), in keeping with the significance of these residues as phosphosites, although these variants do not enhance SlLYK4 function. Collectively, our results indicate that Ser^{320}/Ser^{328}/Ser^{334} in the JM and Ser^{634} in C terminus are required for the function of SlLYK4.

Phosphorylation sites of SlLYK4 differentially regulate EPS and chitin signaling

To investigate the biological significance of SlLYK4 phosphorylation residues in EPS- and chitin-triggered immune responses in planta, we transiently expressed *SlLYK4*, *SlLYK4CD^{km}*, *SlLYK4^{S320A}*, *SlLYK4^{S328A}*, *SlLYK4^{S334A}*, and *SlLYK4^{S634A}* driven by the 35*S* promoter in the roots of *sllyk4-M8* knock mutant background. Similar expression levels of SlLYK4 variants in roots were shown by immunoblotting (fig. S9A). The ROS burst and expression of immune marker genes *SlERF2b*, *SlWRKY3*, and *SlEXO70* were subsequently detected upon EPS and chitin treatment. Similar to SlLYK4^{km}, SlLYK4^{S320A} was unable to restore EPS- and chitin-induced immune marker gene *SlERF2b*, *SlWRKY3*, and *SlEXO70* expression (Fig. 7, A and B, and fig. S9, B and C). SlLYK4^{S334A} failed to complement chitin-induced immune gene induction but completely restored EPS-induced gene expression in *sllyk4-M8* (Fig. 7, A and B, and fig. S9, B and C). Upon chitin and EPS treatment, SlLYK4^{S328A} was abrogated in its ability to restore *SlWRKY3* expression but could recover the *SlERF2b* and *SlEXO70* induction (Fig. 7, A and B, and fig. S9, B and C). Likewise, SlLYK4^{S320A} failed to rescue both EPS- and chitin-induced ROS burst. Nevertheless, SlLYK4^{S334A} and SlLYK^{S328A} complemented the EPS-triggered ROS burst but were unable to rescue ROS accumulation upon chitin induction (Fig. 7, C and D). These data suggested that Ser^{320} residue is critical for SlLYK4 function in both EPS- and chitin-triggered immunity, whereas Ser^{334} exclusively contributes to the chitin signaling and Ser^{328} may regulate only certain branches of the immune responses.

We further analyzed the effect of phosphosite Ser^{634} in SlLYK4 C-terminal domain. SlLYK4^{S634A} expression could not restore EPS-triggered immune marker gene induction in the *sllyk4-M8* mutant; however, chitin-triggered *SlERF2b*, *SlWRKY3*, and *SlEXO70* expression returned to the wild-type level (Fig. 7, A and B, and fig. S9, B and C). Similarly, loss of Ser^{634} phosphorylation impaired the EPS- but not chitin-mediated ROS burst (Fig. 7, E and F) and callose deposition (fig. S9D) in tomato roots. The results suggested that Ser^{634}

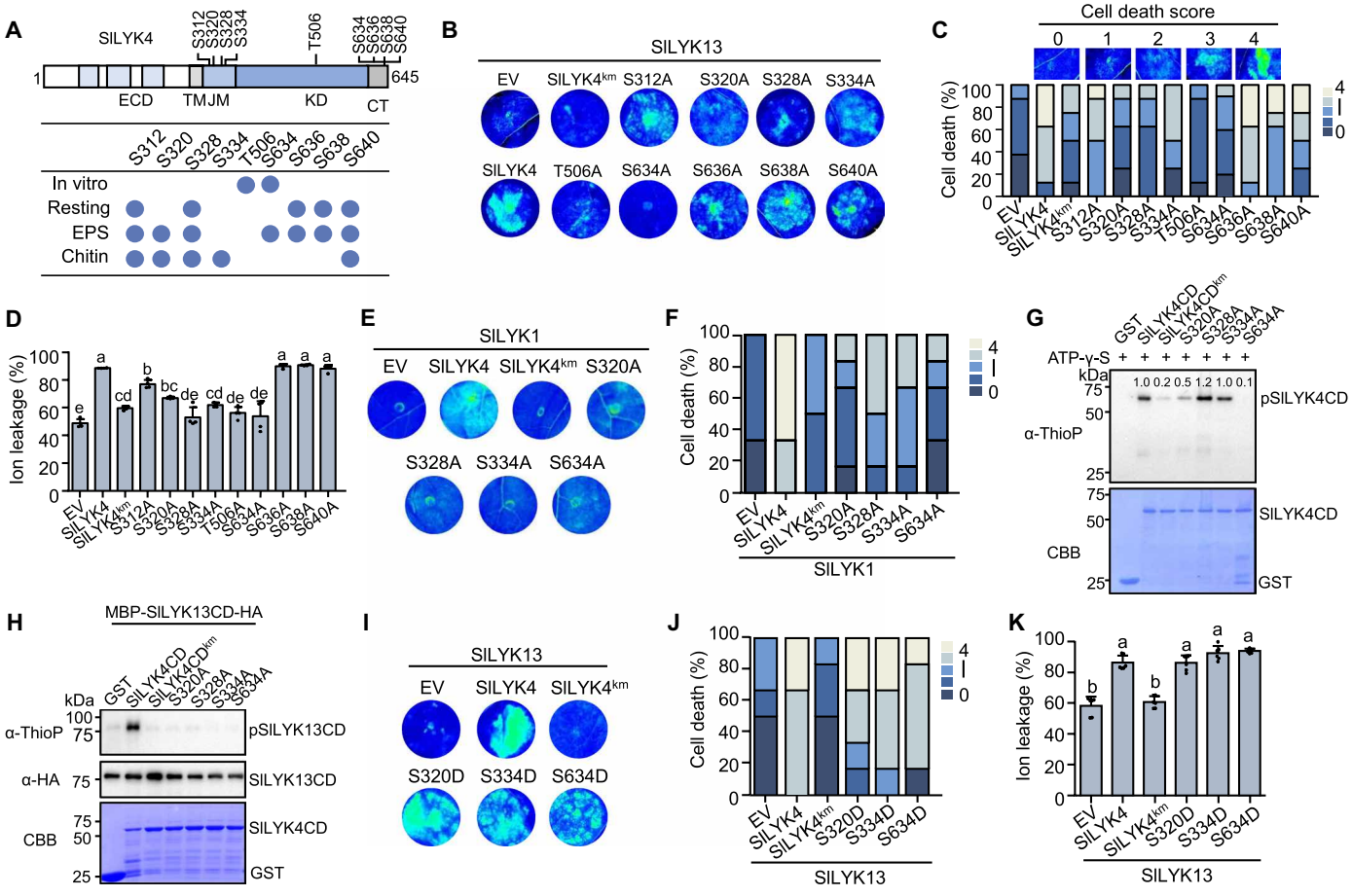

Fig. 6. The phosphorylation residues in the JM and C-terminal domains are essential for SlLYK4 function. (**A**) Phosphorylation sites of SlLYK4 identified in vivo and in vitro by LC-MS/MS analysis. In vitro phosphorylation sites were identified from the kinase assay. For in vivo phosphorylation sites, SlLYK4-FLAG was immunoprecipitated from tomato roots after treatment elicitors. (**B**) Cell death in *N. benthamiana* leaves induced by coexpressing SlLYK13 with SlLYK4 or the phosphosite mutants. Photographs were captured under ultraviolet light after 72 hours. (**C**) Cell death level in *N. benthamiana* leaves induced by coexpressing SlLYK13 with SlLYK4 or the phosphosite mutants. Cell death was scored from eight individual leaves. (**D**) Cell death was quantified by measuring electrolyte leakage. Different letters mean samples with significant differences by one-way ANOVA analysis ($P < 0.05$). Values represent means ± SE ($n = 4$ leaves from different plants). (**E**) Cell death in *N. benthamiana* leaves after coexpression of SlLYK1 with SlLYK4 or the phosphosite mutants for 72 hours. (**F**) Cell death level in (E) was scored from six individual leaves. (**G**) SlLYK4 phosphosite mutants show compromised autophosphorylation. The thiophosphate ester groups were detected by the anti-thiophosphate ester antibody (top). Coomassie blue staining of input proteins is shown. (**H**) The SlLYK4 phosphosite mutants are unable to promote the phosphorylation of SlLYK13. The kinase assay was performed by incubating GST-SlLYK4CD with MBP-SlLYK13CD containing ATP-γ-S. (**I**) Cell death in *N. benthamiana* leaves after coexpression of SlLYK1 with SlLYK4 or the phosphomimetic variants. (**J**) Cell death level in (I) was scored from six individual leaves. (**K**) Cell death in (I) was quantified by measuring electrolyte leakage. Values represent means ± SE ($n = 6$ leaves from different plants). Different letters in [(D) and (K)] mean samples with significant differences by one-way ANOVA analysis ($P < 0.05$). All experiments were performed three times independently with similar results.

phosphorylation is critical for EPS-mediated signaling but indispensable for chitin signaling. To provide evidence for the EPS-induced in vivo phosphorylation of SlLYK4 at Ser^{634}, we generated a specific antibody against the phosphorylated form of SlLYK4 at Ser^{634} (α-pSer^{634}). This antibody was able to exclusively detect the recombination GST-SlLYK4CD protein but not the kinase-dead variants GST-SlLYK4CD^{km} or GST-SlLYK4CD^{S634A} in in vitro kinase assay, suggesting that the specificity of α-pSer^{634} antibody and Ser^{634} is an autophosphorylation residue of SlLYK4 (fig. S9E). By using the anti-pSer^{634} antibody to detect SlLYK4 enriched by immunoprecipitation from *N. benthamiana* leaves, we found that the phosphorylation of Ser^{634} was strongly induced upon EPS but not chitin treatment and was abolished in km or S634A variant (Fig. 7G), indicating that Ser^{634} phosphorylation is stimulated by EPS exclusively in vivo.

To determine the role of Ser^{334} and Ser^{634} residues in resistance to bacterial and fungal pathogens, the hairy root complementary lines in the *sllyk4-M8* mutant background expressing different SlLYK4 variants were infected with *R. solanacearum* or *Fol* by the soil soaking (data S2). We found that the S634A complementary tomatoes were more susceptible to *R. solanacearum*, and the disease index was significantly higher than in the wild-type SlLYK4 complementary tomatoes (Fig. 7, H and I), whereas S334A complementary tomatoes had a similar disease index and survival rate to SlLYK4 complementary plants. Conversely, compromised resistance to *Fol* disease was observed in the S334A complementary tomatoes but not in the S634A

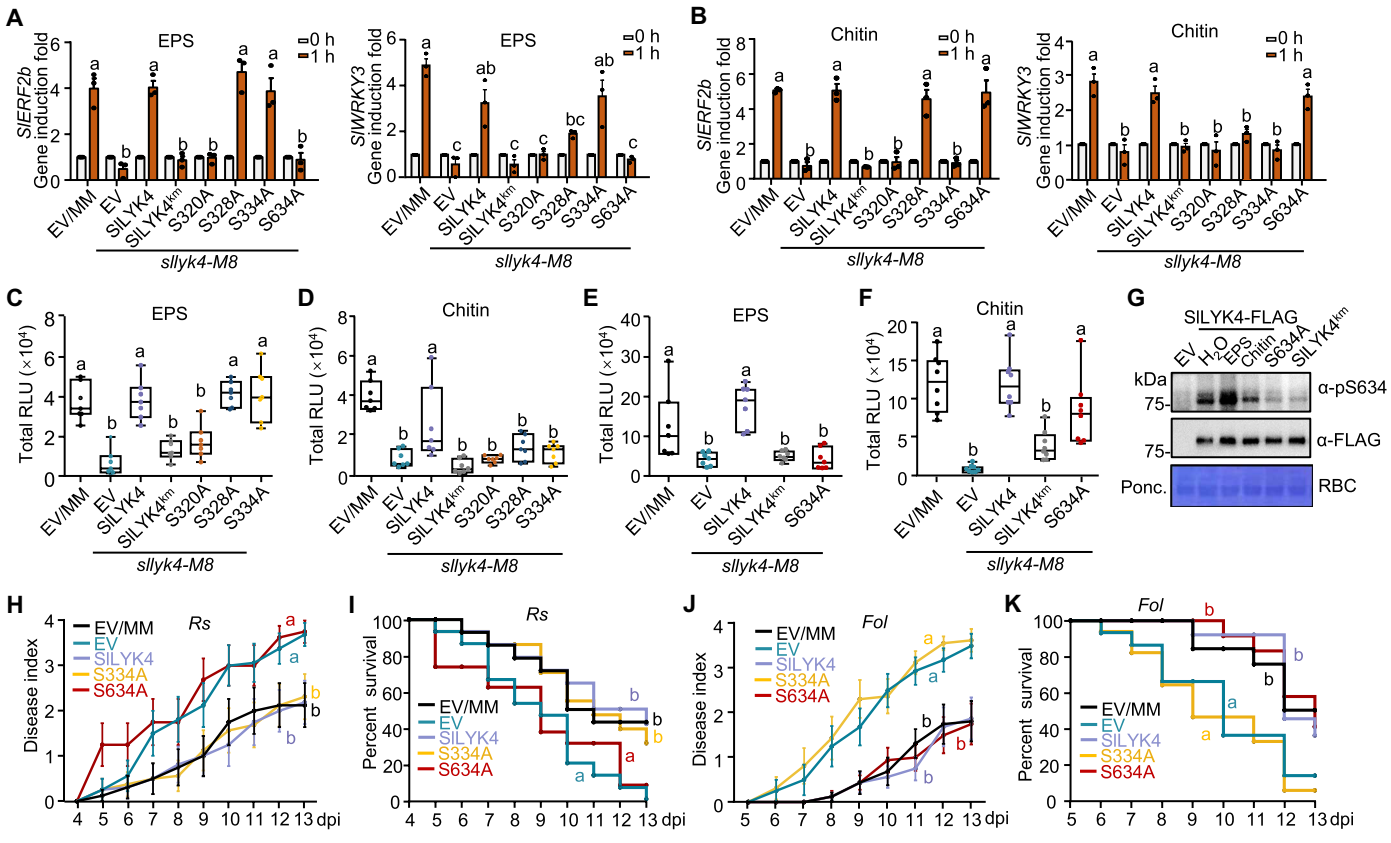

Fig. 7. Different phosphorylation residues of SlLYK4 regulate specificity of immune signaling. (**A**) EPS-induced *SlERF2b* and *SlWRKY3* expression in *sllyk4-M8* roots transiently expressing SlLYK4 and the phospho-variants. (**B**) *SlERF2b* and *SlWRKY3* expression induced by chitin. The roots were treated with EPS (50 μg/ml) or chitin (50 μg/ml) for 1 hour. Values represent the means ± SD ($n = 3$ technical replicates from one biological experiment). (**C** and **D**) ROS burst triggered by EPS or chitin in complementation of *sllyk4-M8* with the indicated SlLYK4 phosphosite mutants. (**E**) Complementation of *sllyk4-M8* with S634A cannot restore EPS-induced ROS burst. (**F**) Complementation of *sllyk4-M8* with S634A restores chitin-induced ROS burst. Measurements in [(C) to (F)] were plotted as box plots displaying all the points, split by the median ($n = 8$). (**G**) SlLYK4 is phosphorylated at Ser^{634} in vivo upon EPS treatment. SlLYK4-FLAG, S634A-FLAG, or $SlLYK4^{km}$ -FLAG was transiently expressed in *N. benthamiana* leaves. Total proteins were analyzed by immunoblot with α-$pSer^{634}$. (**H**) S634A variant cannot restore the resistance defect in the *sllyk4-M8* mutant. Disease index was quantified at the depicted time points ($n = 16$ individual plants, three independent biological repeats; data were showed from one biological experiment). (**I**) Survival ratio was analyzed by comparing the number of survival plants to total plants from the data in (H). (**J**) Complementation of *sllyk4-M8* with S334A showed higher disease index to *Fol*. Disease index was quantified at the depicted time points ($n = 16$ individual plants). (**K**) Survival ratio was analyzed based on the data in (J). Different letters in [(A) to (F)] mean samples with significant differences by one-way ANOVA analysis ($P < 0.05$). In [(H) and (J)], the *P* value was analyzed by a LMM analysis. In [(I) and (K)], the *P* value was analyzed by the log-rank (Mantel-Cox) test. Above experiments were repeated three times independently with similar results. h, hours.

plants (Fig. 7, J and K). Next, we generated $SlLYK4^{km}$ and $SlLYK4^{S634A}$ overexpression plants by hairy root transformation in the susceptible Moneymaker background. Enhanced resistance to bacterial wilt disease was observed in the SlLYK4 overexpression lines, whereas $SlLYK4^{km}$ overexpression lines showed a slight enhancement in resistance (fig. S9, F to H). $SlLYK4^{S634A}$ overexpression lines exhibited comparable resistance, disease index, and survival rate relative to the control lines expressing an empty vector (fig. S9, F to H). Thus, these data indicate that kinase activity and phosphorylation of Ser^{634} are important for SlLYK4 in EPS-triggered bacterial wilt resistance. In summary, our data demonstrate the biological significance of phosphorylation sites of SlLYK4 in differentiating EPS- or chitin-triggered immune signaling and resistance to bacterial or fungal pathogens.

DISCUSSION

Polysaccharide MAMPs from fungal and bacterial pathogens, such as chitin, peptidoglycan, and lipopolysaccharide, all contain a sugar backbone. For example, chitin from fungal cell walls is perceived by the AtLYK5/AtLYK1(AtCERK1) complex in *Arabidopsis* and the OsCEBiP/OsCERK1 complex in rice (*4*, *30*). LjNFR1 and LjNFR5 in *Lotus japonicus* and MtLYK3 and MtNFP in *M. truncatula* are responsible for the identification of Nod factors (lipochitooligosaccharides) (*31*). Although microbial EPS can trigger immune responses in various organisms, the mechanism by which *R. solanacearum* EPS initiates immunity in tomato has remained unexplored. Here, we found that non-RD receptor kinase SlLYK4, belonging to the LysM-RLK IIIA clade, plays a critical role in both EPS and chitin perception in tomato plants (fig. S10). A gene-edited mutant of SlLYK4 completely lost its immune responses that were triggered by EPS. We found that the chitin-mediated immune response was also largely impaired in the SlLYK4 mutant, which is consistent with a recent published finding (*6*). We also demonstrated that the kinase activity of SlLYK4 is vital for its function and identified several key phosphorylation sites of SlLYK4 in the JM and C-terminal domains that are required for the activation

of immune responses. Thus, our study identifies the critical components on the cell membrane for EPS perception.

Further exploration of the co-receptors of SlLYK4 revealed that the RD kinases SlLYK13 mutant abolished EPS-mediated immune response and partial blocked the chitin signaling pathway. In addition, SlLYK1 was also necessary for EPS-triggered immunity, which had previously been reported as a co-receptor for chitin perception in tomato. We propose that SlLYK4 forms a receptor complex with SlLYK13 and SlLYK1 to mediate the recognition of bacterial EPS and fungal chitin (fig. S10). Rice OsCERK1, a widely studied LysM receptor kinase that can participate in multiple signaling pathways, plays an indispensable role in rice recognition of chitin, lipopolysaccharide, peptidoglycan, and Myc factor (*32*–*34*). In tomato, gene duplication has created four orthologs of OsCERK1, namely, SlLYK1 and SlLYK11-13 (*35*). SlLYK12 is mainly expressed in the roots where *Arbuscular mycorrhizal* symbioses are established (*36*). Although both SlLYK1 and SlLYK13 are involved in the signal activation for EPS and chitin, they are not functionally redundant. The mechanisms within the receptor complex are distinct, and their contribution to different MAMP signaling pathways varies. SlLYK13 constantly associates with SlLYK4 independent of EPS or chitin treatment. In contrast, SlLYK1 is recruited into the SlLYK4 complex upon ligand perception. Similarly, Arabidopsis LRR-RLPs interact with AtSOBIR1 in a ligand-independent manner, whereas AtBAK1 is specifically recruited into a preformed RLP-SOBIR1 complex upon ligand perception (*37*, *38*). These findings suggest that SlLYK13 may play a role earlier than SlLYK1 in the very early stage following ligand perception. On the other hand, unlike SlLYK1, which governs both EPS and chitin signaling, SlLYK13 only minimally contributes to chitin signaling. This further confirms that the regulatory mechanism of SlLYK13 is distinct from that of SlLYK1, and their functions are not redundant.

Previous studies have reported that SlLYK1 and SlLYK13 elicit HR responses in *N. benthamiana* leaves, which are dependent on their kinase activities (*36*). The wild-type SlLYK4, but not the kinase-dead mutants K380E and D471N, enhanced cell death when coexpressed with SlLYK1 or SlLYK13. Transient expression of $SlLYK4^{km}$ in Moneymaker roots did not provide resistance to bacterial wilt and could not restore immune defect phenotype of the *sllyk4* mutant. However, $SlLYK4^{km}$ exhibits a stronger interaction with SlLYK1 than the wild-type version in the absence of EPS in *N. benthamiana*. This may be because $SlLYK4^{km}$ is unable to activate immune signaling or because it forms a more stable binding interface. These results supported that the kinase activity and phosphorylation of SlLYK4 are crucial for its biological function. Similarly, kinase activity is required for non-RD receptor FLS2 and NFR5 in immune or mutualistic symbiosis signaling activation (*39*, *40*). However, recent research has shown that EFR kinase activity is dispensable, whereas phosphorylation-dependent conformational changes in the activation loop are essential for the full activation of receptor complex and all elf18-induced immune responses (*41*). Collectively, these findings suggest that non-RD protein kinases exhibit diverse requirements for kinase activity, likely due to their distinct activation mechanisms. We demonstrated that the intracellular domain of SlLYK1 and SlLYK13 can phosphorylate the intracellular domain of SlLYK4 in vitro, but the direct phosphorylation of SlLYK4 on the $SlLYK13CD^{km}$ or $SlLYK1CD^{km}$ variant could not be detected, which may due to the weak kinase activity of SlLYK4. Similarly, the intracellular domain of AtBAK1 can phosphorylate AtEFR, and the intracellular domain of LjNFR1 can phosphorylate LjNFR5, but not vice versa (*40*, *42*). Furthermore, we found that SlLYK4 was able to enhance RD SlLYK13 and SlLYK1 phosphorylation in vitro, which is similar to the function observed in non-RD kinase AtEFR (*43*). The KD of AtEFR undergoes phosphorylation-dependent conformational changes to an active-like state, which would lead to allosteric transactivation of BAK1 by supporting αC-helix positioning (*43*). Similarly, protein interaction analysis conducted using AlphaFold3 revealed that the αC-helix and αE-helix of both SlLYK13 and SlLYK1 are located at the interaction interface with SlLYK4. It would be intriguing to investigate whether the phosphorylation of SlLYK4 could induce a rotation of the αC-helix and αE-helix in SlLYK13 or SlLYK1, thereby directly influencing conformational changes that stabilize the kinase in its active state in future studies.

Given that phosphorylation and kinase activity are both crucial for SlLYK4 in an immune response, we further investigated the important phosphorylation residues of SlLYK4. MS data indicated that a majority of SlLYK4 phosphorylation sites were located in the JM or C-terminal domain. The Ser^{320}, Ser^{328}, and Ser^{334} sites in the JM domain and the Ser^{634} site in the C-terminal domain could not enhance SlLYK13- or SlLYK1-induced cell death in tobacco leaves. Kinase activity analysis of SlLYK4 phosphosite mutants indicated that Ser^{320} and Ser^{634} are important phosphorylation residues for the autophosphorylation of SlLYK4. Furthermore, mutation of all these residues resulted in a loss of ability by SlLYK4CD to enhance SlLYK13CD phosphorylation. Collectively, Ser^{320} and Ser^{634} play an important role in both the autophosphorylation of SlLYK4 and complete activation of the receptor complex, whereas Ser^{328} and Ser^{334} are not required in initial autophosphorylation of SlLYK4. It is also noteworthy that the JM domain plays a critical role in kinase activity for a non-RD receptor kinase. Previous studies have shown that rice OsXA21 and *Arabidopsis* AtBTL2 autophosphorylation sites in the JM domain are critical for kinase activity and biological function (*44*, *45*). The function of the C terminus was more complex. It has been reported that the loss of the AtBAK1 C terminus leads to reduced AtBAK1 autophosphorylation and the C-terminal domain of AtBAK1 inhibits its transphosphorylation activity to AtBRI1 (*46*). Three serine residues, Ser^{602}, Ser^{604}, and Ser^{612}, in the C-terminal domain of AtBAK1 are required for the flg22-mediated immune response (*47*). The C-terminal of AtBRI1 was previously shown to negatively regulate its kinase activity and function (*48*). On the basis of our biochemical and genetic data, phosphorylation of the C-terminal region of SlLYK4 plays a crucial role in EPS signaling.

We observed that both common and specific phosphorylation residues in SlLYK4 could be observed upon EPS or chitin treatments. This raise an important biological question: How can differential phosphorylation occur in response to different ligands while all the components of the receptor complex are the same? On the basis of the working model (fig. S10), the full activation and phosphorylation of SlLYK4 likely result from both its autophosphorylation and transphosphorylation by SlLYK1 and SlLYK13. In the absence of ligands, SlLYK4 forms homodimers or heteromultimers with SlLYK13. Ligand perception induces conformational changes that trigger the autophosphorylation of SlLYK4. Specifically, Ser^{320} in the JM domain, which is essential for kinase activity and both immune pathways, may be phosphorylated during this process. *R. solanacearum* EPS, a high–molecular weight polymer with a network-like structure, which is composed of a diverse array of monosaccharide molecules, differs remarkably from the composition and structure of chitin (*23*). Regions

II and IV in LysM1 of LjNFR1 and LjCERK6 create a structurally defined binding pocket that discriminates between CO8 and Nod factor ligands (*49*). The CD of SlLYK4 likely undergoes distinct conformational changes upon the extracellular domain sensing EPS or chitin, potentially inducing phosphorylation at different sites. Subsequently, the low phosphorylation status of SlLYK4 activates SlLYK13 and recruits SlLYK1, leading to transphosphorylation within the complex and the fully activated SlLYK4. Because SlLYK1 and SlLYK13 are differentially required for EPS or chitin signaling pathway, their transphosphorylation activity may also induce specific phosphorylation residues on SlLYK4.

The tomato SlLYK4 complex is involved in mediating immunity triggered by both EPS and chitin, with the phosphocode of distinct phosphorylation residues playing a pivotal role in initiating different immune pathways. Our findings indicate that Ser^{320} is essential for immunity mediated by both EPS and chitin, whereas Ser^{334} and Ser^{634} are specifically associated with chitin- or EPS-induced signaling, respectively. Although a previous study had reported that many RLK family proteins can function as co-receptors and regulate multiple signaling through distinct phosphorylation sites, the importance of phosphocode for receptors remains poorly understood. AtBAK1 is the common co-receptor for many LRR-type RLKs, and the phosphorylation of Tyr^{403} in the C-terminal domain of AtBAK1 is critical for the flg22-mediated immune response but does not affect BR signal-mediated *Arabidopsis* growth (*47*). AtBRI1-suppressor1 (BSU1), a signaling component in both growth and immunity, transduces brassinosteroid-BRI1 and flagellin-FLS2 signals through different phosphorylation sites (*50*). We found that the phosphorylated peptide sequences containing Ser^{634}, Ser^{636}, Ser^{638}, and Ser^{640} are located at the border region between the KD and the distal C-terminal tail. This region, referred to as the "alpha-I motif" in Symbiosis RLK (SYMRK), has been shown to play a critical role in driving the cellular program leading to root nodule formation. Phosphorylation of the alpha-I motif may create a docking site for downstream components to activate organogenesis (*51*). Ser^{634}, located within the "alpha-I motif" like region, is a critical phosphorylation residue for the autophosphorylation of SlLYK4. We propose that these phosphosites create docking sites for receptor activation, enabling the differentiation of downstream EPS and chitin signaling pathways. The precise regulation of phosphorylation sites provides kinases diverse possibilities to participate in multiple biological processes. As a receptor for multiple MAMPs, SlLYK4 uses distinct phosphorylation regulatory mechanisms across different signaling pathways, allowing the same receptor to discriminate between different MAMPs.

MATERIALS AND METHODS

Plant materials and growth conditions

Solanum lycopersicum cv. Moneymaker, Alisa Craig, and Hawaii 7996 as well as *N. benthamiana* were grown in soil in a growth room at 22°C, 75 μE/m per second (T5 LED Tube Lights, 4000K) with 12-hour light/12-hour dark photoperiod, and 45% relative humidity. *S. lycopersicum* seeds were germinated on half-strength Murashige and Skoog (MS) plates containing 1% (w/v) sucrose and 0.8% (w/v) agar and grown for 10 days. Four-week-old *N. benthamiana* leaves were used for *Agrobacterium*-mediated transformation assays.

Agrobacterium tumefaciens strain GV3101 carrying different constructs were cultured in LB medium with gentamicin (25 mg/ml) and respective antibiotics at 28°C. *R. solanacearum* strains GMI1000 and UW551 were grown on CPG solid medium and cultured at 28°C in CPG liquid medium.

The pathogenic fungal strain *Fol*, strain FGSC 9935, was kindly provided by S. Ouyang from Yangzhou University. *Fol* was grown on potato dextrose agar (PDA) medium for 5 days at 28°C in constant light. Spore suspensions were prepared by harvesting cultures in carboxymethylcellulose sodium medium.

EPS extraction

EPS was extracted from *R. solanacearum* strain GMI1000 and extensively purified according to the method described by McGarvey *et al.* with slight modifications (*52*). GMI1000 was cultured in CPG liquid medium and centrifuged for 15 min at 4000 rpm to obtain bacterial fermentation broth. The cell-free supernatant was lyophilized and redissolved in double-distilled H_2O (ddH_2O). EPS was precipitated overnight at 4°C using 3 volumes of EtOH (v/v) and redissolved in DNase I buffer (50 mM Tris and 1 mM $MgCl_2$). DNase I and RNase A were added and the solution was incubated at 37°C for 1 hour, and proteinase K was added and the solution was incubated at 58°C for 2 hours. Then, the solution was extracted once with phenol, followed by successive extractions with chloroform until no interphase was visible. The aqueous layer was dialyzed extensively against ddH_2O. Pure EPS was recovered from the dialysate by overnight precipitation with 3 volumes of EtOH (v/v) at 4°C. The purified EPS was lyophilized, dissolved in ddH_2O, and frozen in aliquots until use. EPS was quantified by the Elson-Morgan assay for hexosamine sugars using *N*-acetylgalactosamine as the standard.

VIGS assay

Plasmids of binary vectors containing pTRV-RNA1 and pTRV-RNA2 derivatives pTRV2-SlLYKs were transformed into *A. tumefaciens* GV3101. The pTRV2-EV (empty vector) as a negative control and pTRV2-SlPDS (phytoene desaturase) as a positive control were used for monitoring the progress of gene silencing. Agrobacteria were cultivated in LB medium agar plates with corresponding antibiotic for 48 hours at 28°C. Cultures were passaged in fresh medium at a dilution of 1:100 and cultivated for a further 8 hours. After adjusting the concentration to optical density at 600 nm (OD_{600}) = 1.5, each pTRV2 construct was mixed with pTRV1 (1:1) in infiltration buffer [10 mM $MgCl_2$, 10 mM MES, and 200 μM acetosyringone (AS)]. The agrobacterial mix was infiltrated into the abaxial surface of 10-day-old Hawaii 7996 seedlings. Gene silencing efficiency and specificity were determined 4 weeks after agrobacterial infiltration.

CRISPR-Cas9 gene editing

The CRISPR-Cas9 binary vectors (pTX) were derived from pBin19. The target sequence was driven by the tomato *U6* promoter and *Cas9* by 2×35*S*. The recombinant pTX vector was designed to produce insertion or deletions within the coding sequence of SlLYK4, SlLYK13, and SlLYK1 using one single guide RNA (sgRNA) alongside the *Cas9* endonuclease gene (table S1 for guide RNAs used in this study). For genotyping of each first-generation (T1) transgenic line, the guide RNA target sites were amplified by PCR directly from tomato leaf tissue, and the purified PCR products were directly sequenced. Heterozygous and biallelic mutations were identified as overlapping sequence traces near the target. After planting T1 seeds, the T2 transgenic line was obtained for genotype identification, which was similar to T1 plants. The sequences of individual alleles

were determined by sequencing to identify and obtain homozygous edited tomatoes.

Tomato genetic transformation

The tomato transformation assays were performed according to the method described by Zsögön *et al.* with some modifications (*53*). The recombinant vector was introduced into the *A. tumefaciens* strain GV3101 by electroporation, and tomato seeds were surface sterilized and germinated on 1/2 MS medium. Leaf explants (one cotyledon is cut into about two explants, each about 8 mm) were isolated from 2-week-old tomatoes and placed with the abaxial side down onto KCMS medium containing cytokinin (0.1 mg/liter) and 2,4-dichlorophenoxyacetic acid (2,4-D; 1.3 mg/liter) and incubated at 25°C in the dark for 2 days. The explants were immersed in Agrobacterium suspension and mixed gently at room temperature for 3 min. Thereafter, the explants were removed from the suspension and were blotted dry on sterile filter paper and returned to KCMS medium. Plates were maintained in the dark at 25°C for 2 days for cocultivation. After 2 days of cocultivation, explants were transferred to plates with 2 Z medium containing *trans*-zeatin (1 mg/liter), Indole-3-Acetic Acid (IAA; 0.1 mg/liter), timentin (300 mg/liter), and kanamycin (100 mg/liter) for screening and changed the medium every 2 weeks. Some explants may gradually turn white, possibly due to failed infection. Explants that grow healthy callus tissue were isolated to grow adventitious buds and then transferred to 0.2 Z medium containing *trans*-zeatin (0.2 mg/liter), timentin (300 mg/liter), and kanamycin (100 mg/liter) for subculture until strong adventitious buds (2 to 3 cm) develop. Adventitious buds were transferred to rooting medium containing indole-3-butyric acid (IBA; 2 mg/liter), timentin (300 mg/liter), and kanamycin (100 mg/liter) to recover full plants. After the plant has developed a strong root system, it was transplanted to Jiffy Pots for moisture culture for 10 days.

ROS assay

Leaves from 4-week-old tomato plants for each genotype were excised into leaf discs of 0.25 cm^2 and cut into leaf strips, followed by incubation overnight in 96-well plates with 100 μl of ddH_2O to eliminate the wounding effect. The water in the 96-well plate is then sucked out, and 100 μl of reaction solution containing 50 μM luminol and horseradish peroxidase (10 μg/ml) with appropriate elicitors was added, including 100 nM flg22, EPS (50 μg/ml), and chitin (50 μg/ml). Ten-day-old tomato seedlings roots growing on 1/2 MS or 2-week-old transformed tomato roots were cut into 0.5-cm segments, and two root segments were placed in 96-well plates containing 100 μl of ddH_2O for incubation overnight. The water in the 96-well plate is then sucked out, and 100 μl of reaction solution containing 5 μM L-012 and horseradish peroxidase (10 μg/ml) with appropriate elicitors was added. The measurement was carried out promptly after adding the reaction solution with a Multimode Reader Platform (Tecan Austria GmbH, SPARK 10M), measurements were taken every 1.5 min. The values of ROS production represent the relative light units of different plants.

MAPK activation assay

Ten-day-old tomato seedlings growing on 1/2 MS were transferred to the 6-well plate with 1 ml of ddH_2O for overnight recovery. Then, seedlings were treated with chitin (50 μg/ml) for 0, 5, and 15 min; each treatment included three seedlings. The tomato roots were separated from the stems and cotyledon after treatment, and root samples were collected into 1.5-ml tubes. The root samples were then ground in SDS buffer. The supernatant was collected after 12,000 rpm centrifugation for 15 min, and 15-μl protein samples with SDS buffer were loaded on 10% SDS–polyacrylamide gel electrophoresis (SDS-PAGE) gel to detect pMPK3 and pMPK6 by immunoblot with α-pERK1/2 antibody (Cell Signaling Technology, catalog no. 9101).

RNA extraction, reverse transcription, and RT-qPCR

Tomato seedlings growing on 1/2 MS were transferred to the 6-well plate with 1 ml of ddH_2O for overnight recovery. Then, seedlings were treated with EPS (50 μg/ml) for 0, 1, and 3 hours; each treatment included three seedlings. The tomato roots were separated from the stems and cotyledon after treatment. Total RNA was isolated from root samples with TRIzol reagent (TIANGEN, catalog no. DP424). Total RNA (1 μg) was reverse transcribed to synthesize first-strand cDNA at 50°C for 30 min after treatment with RNase-free DNase I at 42°C for 2 min. RT-qPCR analysis was carried out using SYBR Green Supermix with the gene-specific primers (see table S1) on the Analytik Jena qTOWER3G following the standard protocol. The expression of each gene was normalized to the expression of *SlACTIN*.

Callose deposition assay

Tomato seedlings growing on 1/2 MS were transferred to the 6-well plate with 1 ml of ddH_2O for overnight recovery. Then, seedlings were treated with ddH_2O or EPS (50 μg/ml) for 24 hours; each treatment included five biological repeats. The tomato roots were separated from the stems and cotyledon after treatment, and roots were transferred into the fixing solution containing 10% formaldehyde, 5% acetic acid, and 50% ethanol for 12 hours. The roots were washed twice with 75% ethanol and three times with ddH_2O water and then dipped in 0.01% aniline blue solution (150 mM KH_2PO_4, pH 9.5) for 15 min for callose staining. The roots were fixed to the slides using 50% glycerin, and callose deposition was detected with a fluorescence microscope (Leica, DM2500).

Phylogenetic analysis of LysM-RLKs

The gene information and database source of the LysM-RLKs are shown in table S2. The phylogenetic tree was generated with MEGA11.0 software using the maximum likelihood method based on the Le_Gascuel model (*54*). Initial tree(s) for the heuristic search were obtained automatically by applying Neighbor-Join and BioNJ algorithms to a matrix of pairwise distances estimated using a JTT model and then selecting the topology with superior log likelihood value. A discrete gamma distribution was used to model evolutionary rate differences among sites. The percentage of replicate trees in which the associated taxa clustered together in the bootstrap test (1000 replicates) is shown next to the branches.

A. rhizogenes–mediated tomato root transformation

The tomato transformation assays were performed according to the method described by Ho-Plágaro *et al.* with slight modifications (*55*). *A. rhizogenes* MSU440 containing the corresponding overexpression vector was used to transform *S. lycopersicum* plantlets. *S. lycopersicum* seeds were surface sterilized by soaking for 5 min using 70% alcohol and 2.35% (w/v) sodium hypochlorite [50% (v/v) commercial bleach] and then washed three times with sterile distilled

water. *S. lycopersicum* seeds were germinated on half-strength MS plates and grown for 10 days. To generate hairy roots, the radicle and the bottom part of the hypocotyl from these 10-day-old seedlings were removed. The hypocotyl incision was dipped into a single *A. rhizogenes* colony for 3 s. These wounded seedlings were kept on the same half-strength MS agar plates, and their hypocotyls were covered with a humid filter paper strip to maintain moisture. The seedlings were left to root in a growth chamber under the same conditions as before. Roots grown during the first week (adventitious laterals, nontransformed roots) were removed, and plantlets were transferred to half-strength MS agar medium with kanamycin (50 mg/ml). After 2 weeks, the protein expression in the roots was detected by immunoblot with α-HA antibody (Roche, catalog no. 12013819001). Positive transformed tomatoes will be tested for ROS burst or transferred to Jiffy Pots and allowed to grow in a growth room. After 3 weeks of growth, *R. solanacearum* inoculation experiment will be carried out.

Pathogen inoculation assay

All the *R. solanacearum* infection assays were inoculated by irrigating root inoculation. Four-week-old tomato planted in 4.5-cm square Jiffy Pots were soaked in *R. solanacearum* suspension with OD_{600} = 0.1 for 1 hour. The plants were kept in a growth incubator at 75% humidity, 12-hour light/12-hour dark photoperiod, and 28°C for disease symptom scoring. The visual disease symptoms of each plant was scored on the basis of a 0 to 4 disease index scale (*56*), where 0 represented no symptoms, 1 corresponded to 1 to 25% leaf area wilting, 2 for 26 to 49%, 3 for 50 to 74%, and 4 for complete wilting. For bacteria quantification in tomato stems, 0.25-g tissues above the stem base were ground in ddH_2O and the diluted solution was spread on solid CPG medium with appropriate antibiotics; CFUs (colony-forming units) were counted after 2 days culture at 28°C.

Fol strain FGSC 9935 was grown on PDA medium for 5 days at 28°C. Spore suspensions were prepared by harvesting cultures in carboxymethylcellulose sodium medium at a concentration of 10^{-6} spores/ml. Two-week-old tomato seedlings planted in 4.5-cm square Jiffy Pots were inoculated with 20 ml of *Fol* spores and kept in a growth incubator at 75% humidity, 12-hour light/12-hour dark photoperiod, and 28°C for disease symptom scoring. The grades of tomato fungal wilt disease as described by Ouyang *et al.* (*57*).

N. benthamiana leaf transient assays

A. tumefaciens strain GV3101 harboring indicated binary constructs were streaked on selective LB medium agar plates and grown for 48 hours. Cultures were grown in liquid LB medium overnight at 28°C in a shaking incubator. Cells were harvested by centrifugation for 5 min at 4000 rpm and resuspended in Agrobacterium infiltration buffer containing 10 mM $MgCl_2$, 10 mM MES, and 200 μM AS at the density of OD_{600} = 1.5. Leaf sections of 4-week-old *N. benthamiana* fully expanded leaves were infiltrated with a 1-ml needleless syringe.

Co-IP assay

Four-week-old *N. benthamiana* leaves were infiltrated with *A. tumefaciens* (strain GV3101). Thirty-six hours after infiltration, leaves were treated with water (as control) or a solution containing EPS (50 μg/ml) for 15 min. Twenty-five leaf discs of 0.25 cm^2 were injected with different Agrobacterium. The leaves were ground and lysed with Co-IP buffer containing 20 mM tris-HCl (pH 7.5), 100 mM NaCl, 1 mM EDTA, 2 mM dithiothreitol (DTT), 10% glycerol, 0.5% Triton X-100, and protease inhibitor cocktail (Roche, catalog no. 04693116001). The supernatant was collected after 12,000 rpm centrifugation for 15 min. Immunoprecipitation was performed with 6 μl of FLAG-trap beads (Sigma-Aldrich, catalog no. A2220) with 3-hour incubation at 4°C. Beads were washed five times with washing buffer containing 20 mM tris-HCl (pH 7.5), 100 mM NaCl, 1 mM EDTA, and 0.1% Triton X-100. The proteins were stripped from the beads by heating in SDS buffer for 10 min at 95°C. The immunoprecipitated proteins and input proteins were separated on SDS-PAGE gels for Western blot analysis with the indicated antibodies.

BiFC assay

The plasmids were introduced into *A. tumefaciens*. Four-week-old *N. benthamiana* leaves were infiltrated with *A. tumefaciens* containing the corresponding plasmid. Venus fluorescence signals in the *N. benthamiana* leaf discs were examined at ~36 hours with confocal microscopy (Leica, SP8). Yellow fluorescence protein was excited at 514 nm, and the emission was collected between 524 and 550 nm. Images were captured and analyzed by the Leica Application Suite X (LAS X) software platform.

Yeast two-hybrid assay

Intracellular KDs of SlLYK4 and SlLYK13 were cloned into pBK and pAD vectors, respectively, which were then introduced into yeast cells. Cotransformed yeast cells were screened on synthetic dropout media lacking leucine and tryptophan (SD/-Leu-Trp). The single yeast colonies were serially diluted onto SD/-Leu-Trp and SD/-Leu-Trp-His with 3-amino-1,2,4-triazole (3-AT) (500 mM) to observe yeast cell growth.

In vitro pull-down and kinase assay

Fusion proteins from vector pGST or pMAL were expressed in the *E. coli* BL21 strain and purified through affinity chromatography with glutathione agarose or amylose resin. For pull-down assay, MBP-SlLYK1CD or MBP-SlLYK13CD fusion proteins (tagged with HA) were preincubated with 5 μl of prewashed glutathione agarose in 300 μl of incubation buffer [20 mM tris-HCl (pH 7.5), 100 mM NaCl, 0.1 mM EDTA, and 0.5% Triton X-100] for 0.5 hours at 4°C. After centrifugation, the supernatant was collected and incubated with GST or GST-SlLYK4CD beads for another 1 hour. Then, the agarose was spun down and washed three times with washing buffer [20 mM tris-HCl (pH 7.5), 300 mM NaCl, 0.1 mM EDTA, and 0.1% Triton X-100]. The pull-down proteins were detected with an α-HA antibody by immunoblot, and α-GST antibody (Abmart, M20007; 1:5000) was used to detect the loading of GST or GST- SlLYK4CD proteins.

For in vitro kinase assay, the kinase (1 μg) and substrate (5 μg) were mixed in kinase buffer [25 mM Hepes (pH 7.5), 10 mM $MgCl_2$, 2 mM $MnCl_2$, and 1 mM DTT] with 0.1 mM cold ATP at 28°C for 3 hours. The phosphorylation of fusion proteins was analyzed by anti-pThr/Tyr (Cell Signaling Technology, catalog no. 9381S) after separation with 10% SDS-PAGE. For in vitro phosphorylation assays followed by *p*-nitrobenzyl mesylate (PNBM) alkylation, the kinase (1 μg) and substrate (5 μg) were mixed in kinase buffer with 1.5 mM ATP-γ-S (Abcam, ab138911) at 28°C for 3 hours. After adding 1.5 μl of 50 mM PNBM (Abcam, ab138910), the samples were incubated at 28°C for 1.5 hours. Recombinant proteins were separated by 10% (w/v) SDS-PAGE, and phosphorylated proteins were detected by immunoblotting with anti-thiophosphate ester antibody (Abcam, ab92570; 1:10,000).

Cell death in *N. benthamiana* and ion leakage assay

N. benthamiana leaves were infiltrated with *A. tumefaciens* containing the corresponding plasmid. Images of the leaves of *N. benthamiana* were captured under bright light and ultraviolet light at 72 hours after infiltration. For electrolyte leakage measurements, six leaf discs of 0.25 cm^2 from infiltrated *N. benthamiana* leaf areas were sampled and floated on 5 ml of ddH_2O for 5 hours at room temperature (five leaf discs/tuber). Then, the conductivity in the solution was measured using an electrical conductivity meter (METTLER TOLEDO FiveGo F3) and the tubes were put in the boiling water and boiled for 20 min. Total conductivity was measured after the solution cooled to room temperature. The electrolyte leakage was expressed by the ratio of the conductivity to the total conductivity.

MS analysis

In vitro phosphorylation for MS analysis was performed in a 30-μl reaction for 2 hours at room temperature. The reaction buffer contains 20 mM tris-HCl (pH 7.5), 10 mM $MgCl_2$, 5 mM EDTA, 1 mM DTT, 0.1 mM ATP, and 10 μg of GST-SlLYK4CD with or without 10 μg of MBP-SlLYK13CD. The phosphorylated GST-SlLYK4CD proteins were resolved by 10% SDS-PAGE gel. To identify EPS- or chitin-induced phosphorylation sites in vivo, we transiently expressed SlLYK4-FLAG in tomato hairy roots for 2 weeks and treated samples with EPS (50 μg/ml) or chitin (50 μg/ml) for 15 min. About 6 g of homogenized tissues was lysed in 40 ml of Co-IP buffer, and proteins were immunoprecipitated with 60 μl of anti-Flag affinity gel (Bimake) at 4°C for 3 hours. The enriched SlLYK4-FLAG proteins were resolved by 10% SDS-PAGE gel, and the gel was visualized by Coomassie brilliant blue (CBB) staining. The corresponding bands were sliced and subjected to in-gel digestion with trypsin.

Phosphosites analysis were performed on a nanoflow EASY-nLC1000 system connected to an Orbitrap Q Exactive (Thermo Fisher Scientific, Bremen, Germany) equipped with a nanoelectrospray source by PTM Biolab Company (Hangzhou, China). The analytical conditions were as follows: Each sample was loaded by an autosampler and separated on a 15-cm analytical column (75 μm inner diameter) packed with 3-μm C18 beads. Separation is performed using a 10 to 40% Acetonitrile gradient (200 min) with 0.1% formic acid at a flow rate of 300 μl/min. MS samples were analyzed using Mascot (Matrix Science; version 2.3.0) and MaxQuant (version 1.6.6). The MS spectrums and B and Y ion information for all phosphorylation residues are provided in data S1.

Phosphopeptide antibody preparation

Phosphopeptide antibodies were generated at Abmart (China). The phosphopeptides HSWET (pS)FSTS and corresponding control peptides HSWETSFSTS was synthesized for making phosphopeptide-specific antibodies to recognize the Ser^{634} phosphorylation of SlLYK4. Two rabbits were immunized with the phosphopeptide conjugated to a keyhole limpet hemocyanin carrier. The polyclonal antiserum was purified from the first by affinity chromatography using phosphopeptides, and the eluate was passed through a second column with the control peptides to remove nonspecific antibodies. The Ser^{634} phosphopeptide antibody (1.0 μg/ml) was used in in vitro kinase assays.

Immunoprecipitation assay

SlLYK4-FLAG was transiently expressed in *N. benthamiana* leaves for 24 hours, and samples were treated with EPS (50 μg/ml). Three grams of homogenized tissues in liquid nitrogen was lysed in 30 ml of Co-IP buffer, and proteins were immunoprecipitated with 30 μl of anti-Flag affinity gel (Bimake) at 4°C for 3 hours. The beads were washed three times with 1 ml of washing buffer and were boiled at 95°C for 10 min with 50 μl of 2× SDS-PAGE loading buffer. The boiled beads were centrifuged at 12,000 rpm for 1 min. Then, the enriched SlLYK4-FLAG proteins were resolved by 10% SDS-PAGE gel and used to analyze Ser^{634} phosphorylation with anti-$pSer^{634}$ and the anti-$pSer^{634}$ antibody (10.0 μg/ml) was used in 5% bovine serum albumin in Tris-buffered saline with Tween 20 (TBST).

Statistical analysis

Statistical analysis was conducted with the software of GraphPad Prism 8.0 using one-way analysis of variance (ANOVA) with Tukey's multiple comparisons test or using two-tailed Student's *t* test. Different letters indicate significant differences with $P < 0.05$. n.s. indicates no significant difference. In the statistics of *R. solanacearum* inoculation, the area under the disease progression curve (AUDPC) in was calculated by a linear mixed effect model (LMM) analysis with Tukey's post hoc test for multiple comparisons by R as previously described (*58*). Survival ratio was analyzed by comparing the number of survival plants to total plants. The Kaplan-Meier estimates survival analysis was performed by the log-rank (Mantel-Cox) test with Tukey's post hoc test for multiple comparisons and Bonferroni adjusted by R (*58*). Statistical details can be found in the figure legends.

Supplementary Materials

The PDF file includes:

Figs. S1 to S10
Tables S1 to S3
Legends for data S1 and S2

Other Supplementary Material for this manuscript includes the following:

Data S1 and S2

REFERENCES AND NOTES

1. F. Boutrot, C. Zipfel, Function, discovery, and exploitation of plant pattern recognition receptors for broad-spectrum disease resistance. *Annu. Rev. Phytopathol.* **55**, 257–286 (2017).
2. M. Cai, H. Yu, E. Sun, C. Zuo, Receptor-like proteins: Decision-makers of plant immunity. *Phytopathol. Res.* **6**, 58 (2024).
3. C. Zipfel, Plant pattern-recognition receptors. *Trends Immunol.* **35**, 345–351 (2014).
4. Y. Cao, Y. Liang, K. Tanaka, C. T. Nguyen, R. P. Jedrzejczak, A. Joachimiak, G. Stacey, The kinase LYK5 is a major chitin receptor in *Arabidopsis* and forms a chitin-induced complex with related kinase CERK1. *Elife* **3**, e03766 (2014).
5. H. Kaku, Y. Nishizawa, N. Ishii-Minami, C. Akimoto-Tomiyama, N. Dohmae, K. Takio, E. Minami, N. Shibuya, Plant cells recognize chitin fragments for defense signaling through a plasma membrane receptor. *Proc. Natl. Acad. Sci. U.S.A.* **103**, 11086–11091 (2006).
6. Y. Ai, Q. Li, C. Li, R. Wang, X. Sun, S. Chen, X.-Z. Cai, X. Qi, Y. Liang, Tomato LysM receptor kinase 4 mediates chitin-elicited fungal resistance in both leaves and fruit. *Hortic. Res.* **10**, uhad082 (2023).
7. X. Yu, B. Feng, P. He, L. Shan, From chaos to harmony: Responses and signaling upon microbial pattern recognition. *Annu. Rev. Phytopathol.* **55**, 109–137 (2017).
8. J. D. G. Jones, J. L. Dangl, The plant immune system. *Nature* **444**, 323–329 (2006).
9. L. Pi, Y. Zhang, J. Wang, N. Wang, Z. Yin, D. Dou, A G-type lectin receptor-like kinase in *Nicotiana benthamiana* enhances resistance to the fungal pathogen *Sclerotinia sclerotiorum* by complexing with CERK1/LYK4. *Phytopathol. Res.* **5**, 27 (2023).
10. C. Dardick, B. Schwessinger, P. Ronald, Non-arginine-aspartate (non-RD) kinases are associated with innate immune receptors that recognize conserved microbial signatures. *Curr. Opin. Plant Biol.* **15**, 358–366 (2012).
11. B. Simonsen, H. Rübsam, M. V. Kolte, M. M. Larsen, C. Krönauer, K. Gysel, M. Laursen, F. Feng, G. Kaya, G. E. D. Oldroyd, J. Stougaard, S. Fort, S. Radutoiu, K. R. Andersen, The *Medicago truncatula* LYR4 intracellular domain serves as a scaffold in immunity signaling

independent of its phosphorylation activity. bioRxiv 2024.10.23.619817 [Preprint] (2024). https://doi.org/10.1101/2024.10.23.619817.
12. D. Tang, G. Wang, J.-M. Zhou, Receptor kinases in plant-pathogen interactions: More than pattern recognition. *Plant Cell* **29**, 618–637 (2017).
13. T. Denny, "Plant pathogenic Ralstonia species" in *Plant-associated bacteria*, S. S. Gnanamanickam, Ed. (Springer Netherlands, 2006), chap. 16, pp. 573–644.
14. T. M. Lowe-Power, D. Khokhani, C. Allen, How *Ralstonia solanacearum* exploits and thrives in the flowing plant xylem environment. *Trends Microbiol.* **26**, 929–942 (2018).
15. S. Genin, T. P. Denny, Pathogenomics of the *Ralstonia solanacearum* species complex. *Annu. Rev. Phytopathol.* **50**, 67–89 (2012).
16. D. Landry, M. González-Fuente, L. Deslandes, N. Peeters, The large, diverse, and robust arsenal of *Ralstonia solanacearum* type III effectors and their in planta functions. *Mol. Plant Pathol.* **21**, 1377–1388 (2020).
17. C. Pfund, J. Tans-Kersten, F. M. Dunning, J. M. Alonso, J. R. Ecker, C. Allen, A. F. Bent, Flagellin is not a major defense elicitor in *Ralstonia solanacearum* cells or extracts applied to *Arabidopsis thaliana*. *Mol. Plant Microbe Interact.* **17**, 696–706 (2004).
18. G. Kunze, C. Zipfel, S. Robatzek, K. Niehaus, T. Boller, G. Felix, The N terminus of bacterial elongation factor Tu elicits innate immunity in Arabidopsis plants. *Plant Cell* **16**, 3496–3507 (2004).
19. L. Wang, M. Albert, E. Einig, U. Furst, D. Krust, G. Felix, The pattern-recognition receptor CORE of Solanaceae detects bacterial cold-shock protein. *Nat. Plants* **2**, 16185 (2016).
20. Y. Wei, C. Caceres-Moreno, T. Jimenez-Gongora, K. Wang, Y. Sang, R. Lozano-Duran, A. P. Macho, The *Ralstonia solanacearum* csp22 peptide, but not flagellin-derived peptides, is perceived by plants from the *Solanaceae* family. *Plant Biotechnol. J.* **16**, 1349–1362 (2018).
21. J. Ke, W. Zhu, Y. Yuan, X. Du, A. Xu, D. Zhang, S. Cao, W. Chen, Y. Lin, J. Xie, J. Cheng, Y. Fu, D. Jiang, X. Yu, B. Li, Duality of immune recognition by tomato and virulence activity of the Ralstonia solanacearum exo-polygalacturonase PehC. *Plant Cell* **35**, 2552–2569 (2023).
22. E. Saile, J. A. McGarvey, M. A. Schell, T. P. Denny, Role of extracellular polysaccharide and endoglucanase in root invasion and colonization of tomato plants by *Ralstonia solanacearum*. *Phytopathology* **87**, 1264–1271 (1997).
23. G. Orgambide, H. Montrozier, P. Servin, J. Roussel, D. Trigaletdemery, A. Trigalet, High heterogeneity of the exopolysaccharides of *Pseudomonas solanacearum* strain GMI 1000 and the complete structure of the major polysaccharide. *J. Biol. Chem.* **266**, 8312–8321 (1991).
24. Y. Mori, Y. Hosoi, S. Ishikawa, K. Hayashi, Y. Asai, H. Ohnishi, M. Shimatani, K. Inoue, K. Ikeda, H. Nakayashiki, Y. Nishimura, K. Ohnishi, A. Kiba, K. Kai, Y. Hikichi, Ralfuranones contribute to mushroom-type biofilm formation by *Ralstonia solanacearum* strain OE1-1. *Mol. Plant Pathol.* **19**, 975–985 (2018).
25. A. Milling, L. Babujee, C. Allen, *Ralstonia solanacearum* extracellular polysaccharide is a specific elicitor of defense responses in wilt-resistant tomato plants. *PLOS ONE* **6**, e15853 (2011).
26. A. Prakasha, I. D. Grice, K. S. V. Kumar, M. P. Sadashiva, H. N. Shankar, S. Umesha, Extracellular polysaccharide from *Ralstonia solanacearum*; A strong inducer of eggplant defense against bacterial wilt. *Biol. Control* **110**, 107–116 (2017).
27. T. Sakamoto, M. Deguchi, O. J. B. Brustolini, A. A. Santos, F. F. Silva, E. P. B. Fontes, The tomato RLK superfamily: Phylogeny and functional predictions about the role of the LRRII-RLK subfamily in antiviral defense. *BMC Plant Biol.* **12**, 229 (2012).
28. L. Yan, Y. Ma, D. Liu, X. Wei, Y. Sun, X. Chen, H. Zhao, J. Zhou, Z. Wang, W. Shui, Z. Lou, Structural basis for the impact of phosphorylation on the activation of plant receptor-like kinase BAK1. *Cell Res.* **22**, 1304–1308 (2012).
29. D. P. Lu, S. J. Wu, X. Q. Gao, Y. L. Zhang, L. B. Shan, P. He, A receptor-like cytoplasmic kinase, BIK1, associates with a flagellin receptor complex to initiate plant innate immunity. *Proc. Natl. Acad. Sci. U.S.A.* **107**, 496–501 (2010).
30. T. Shimizu, T. Nakano, D. Takamizawa, Y. Desaki, N. Ishii-Minami, Y. Nishizawa, E. Minami, K. Okada, H. Yamane, H. Kaku, N. Shibuya, Two LysM receptor molecules, CEBiP and OsCERK1, cooperatively regulate chitin elicitor signaling in rice. *Plant J.* **64**, 204–214 (2010).
31. E. Limpens, C. Franken, P. Smit, J. Willemse, T. Bisseling, R. Geurts, LysM domain receptor kinases regulating rhizobial Nod factor-induced infection. *Science* **302**, 630–633 (2003).
32. Y. Ao, Z. Li, D. Feng, F. Xiong, J. Liu, J.-F. Li, M. Wang, J. Wang, B. Liu, H.-B. Wang, OsCERK1 and OsRLCK176 play important roles in peptidoglycan and chitin signaling in rice innate immunity. *Plant J.* **80**, 1072–1084 (2014).
33. Y. Desaki, Y. Kouzai, Y. Ninomiya, R. Iwase, Y. Shimizu, K. Seko, A. Molinaro, E. Minami, N. Shibuya, H. Kaku, Y. Nishizawa, OsCERK1 plays a crucial role in the lipopolysaccharide-induced immune response of rice. *New Phytol.* **217**, 1042–1049 (2018).
34. J. He, C. Zhang, H. Dai, H. Liu, X. Zhang, J. Yang, X. Chen, Y. Zhu, D. Wang, X. Qi, W. Li, Z. Wang, G. An, N. Yu, Z. He, Y.-F. Wang, Y. Xiao, P. Zhang, E. Wang, A LysM receptor heteromer mediates perception of arbuscular mycorrhizal symbiotic signal in rice. *Mol. Plant* **12**, 1561–1576 (2019).
35. L. Buendia, A. Girardin, T. Wang, L. Cottret, B. Lefebvre, LysM receptor-like kinase and LysM receptor-like protein families: An update on phylogeny and functional characterization. *Front. Plant Sci.* **9**, 1531 (2018).
36. D. Liao, X. Sun, N. Wang, F. Song, Y. Liang, Tomato LysM receptor-like kinase SlLYK12 is involved in arbuscular mycorrhizal symbiosis. *Front. Plant Sci.* **9**, 1004 (2018).
37. I. Albert, H. Böhm, M. Albert, C. E. Feiler, J. Imkampe, N. Wallmeroth, C. Brancato, T. M. Raaymakers, S. Oome, H. Zhang, E. Krol, C. Grefen, A. A. Gust, J. Chai, R. Hedrich, G. Van den Ackerveken, T. Nürnberger, An RLP23-SOBIR1-BAK1 complex mediates NLP-triggered immunity. *Nat. Plants* **1**, 15140 (2015).
38. E. Domazakis, D. Wouters, R. G. F. Visser, S. Kamoun, M. H. A. J. Joosten, V. G. A. A. Vleeshouwers, The ELR-SOBIR1 complex functions as a two-component receptor-like kinase to mount defense against *Phytophthora infestans*. *Mol. Plant Microbe Interact.* **31**, 795–802 (2018).
39. Y. Cao, D. J. Aceti, G. Sabat, J. Song, S.-i. Makino, B. G. Fox, A. F. Bent, Mutations in FLS2 Ser-938 dissect signaling activation in FLS2-mediated Arabidopsis immunity. *PLOS Pathog.* **9**, e1003313 (2013).
40. E. B. Madsen, M. Antolín-Llovera, C. Grossmann, J. Ye, S. Vieweg, A. Broghammer, L. Krusell, S. Radutoiu, O. N. Jensen, J. Stougaard, M. Parniske, Autophosphorylation is essential for the in vivo function of the *Lotus japonicus* Nod factor receptor 1 and receptor-mediated signalling in cooperation with Nod factor receptor 5. *Plant J.* **65**, 404–417 (2011).
41. K. W. Bender, D. Couto, Y. Kadota, A. P. Macho, J. Sklenar, P. Derbyshire, M. Bjornson, T. A. DeFalco, A. Petriello, M. F. Farre, B. Schwessinger, V. Ntoukakis, L. Stransfeld, A. M. E. Jones, F. L. H. Menke, C. Zipfel, Activation loop phosphorylaton of a non-RD receptor kinase initiates plant innate immune signaling. *Proc. Natl. Acad. Sci. U.S.A.* **118**, e2108242118 (2021).
42. B. Schwessinger, M. Roux, Y. Kadota, V. Ntoukakis, J. Sklenar, A. Jones, C. Zipfel, Phosphorylation-dependent differential regulation of plant growth, cell death, and innate immunity by the regulatory receptor-like kinase BAK1. *PLOS Genet.* **7**, e1002046 (2011).
43. H. Müehlenbeck, Y. Tsutsui, M. A. Lemmon, K. W. Bender, C. Zipfel, Allosteric activation of the co-receptor BAK1 by the EFR receptor kinase initiates immune signaling. *Elife* **12**, RP92110 (2024).
44. X. Chen, M. Chern, P. E. Canlas, C. Jiang, D. Ruan, P. Cao, P. C. Ronald, A conserved threonine residue in the juxtamembrane domain of the XA21 pattern recognition receptor is critical for kinase autophosphorylation and XA21-mediated immunity. *J. Biol. Chem.* **285**, 10454–10463 (2010).
45. X. Yu, Y. Xie, D. Luo, H. Liu, M. V. V. de Oliveira, P. Qi, S.-I. Kim, F. A. Ortiz-Morea, J. Liu, Y. Chen, S. Chen, B. Rodrigues, B. Li, S. Xue, P. He, L. Shan, A phospho-switch constrains BTL2-mediated phytocytokine signaling in plant immunity. *Cell* **186**, 2329–2344.e20 (2023).
46. D. Wu, Y. Liu, F. Xu, Y. Zhang, Differential requirement of BAK1 C-terminal tail in development and immunity. *J. Integr. Plant Biol.* **60**, 270–275 (2018).
47. A. Perraki, T. A. DeFalco, P. Derbyshire, J. Avila, D. Séré, J. Sklenar, X. Qi, L. Stransfeld, B. Schwessinger, Y. Kadota, A. P. Macho, S. Jiang, D. Couto, K. U. Torii, F. L. H. Menke, C. Zipfel, Phosphocode-dependent functional dichotomy of a common co-receptor in plant signalling. *Nature* **561**, 248–252 (2018).
48. X. Wang, X. Li, J. Meisenhelder, T. Hunter, S. Yoshida, T. Asami, J. Chory, Autoregulation and homodimerization are involved in the activation of the plant steroid receptor BRI1. *Dev. Cell* **8**, 855–865 (2005).
49. Z. Bozsoki, K. Gysel, S. B. Hansen, D. Lironi, C. Krönauer, F. Feng, N. de Jong, M. Vinther, M. Kamble, M. B. Thygesen, E. Engholm, C. Kofoed, S. Fort, J. T. Sullivan, C. W. Ronson, K. J. Jensen, M. Blaise, G. Oldroyd, J. Stougaard, K. R. Andersen, S. Radutoiu, Ligand-recognizing motifs in plant LysM receptors are major determinants of specificity. *Science* **369**, 663–670 (2020).
50. C. H. Park, Y. Bi, J. H. Youn, S. H. Kim, J. G. Kim, N. Y. Xu, R. Shrestha, A. L. Burlingame, S. L. Xu, M. B. Mudgett, S. K. Kim, T. W. Kim, Z. Y. Wang, Deconvoluting signals downstream of growth and immune receptor kinases by phosphocodes of the BSU1 family phosphatases. *Nat. Plants* **8**, 646–655 (2022).
51. N. B. Abel, M. M. M. Nørgaard, S. B. Hansen, K. Gysel, I. A. Díez, O. N. Jensen, J. Stougaard, K. R. Andersen, Phosphorylation of the alpha-I motif in SYMRK drives root nodule organogenesis. *Proc. Natl. Acad. Sci. U.S.A.* **121**, e2311522121 (2024).
52. J. A. McGarvey, T. P. Denny, M. A. Schell, Spatial-temporal and quantitative analysis of growth and EPS I production by *Ralstonia solanacearum* in resistant and susceptible tomato cultivars. *Phytopathology* **89**, 1233–1239 (1999).
53. A. Zsögön, T. Čermák, E. R. Naves, M. M. Notini, K. H. Edel, S. Weinl, L. Freschi, D. F. Voytas, J. Kudla, L. E. P. Peres, De novo domestication of wild tomato using genome editing. *Nat. Biotechnol.* **36**, 1211–1216 (2018).
54. K. Tamura, G. Stecher, S. Kumar, MEGA11 molecular evolutionary genetics analysis version 11. *Mol. Biol. Evol.* **38**, 3022–3027 (2021).
55. T. Ho-Plágaro, R. Huertas, M. I. Tamayo-Navarrete, J. A. Ocampo, J. M. García-Garrido, An improved method for *Agrobacterium rhizogenes*-mediated transformation of tomato suitable for the study of arbuscular mycorrhizal symbiosis. *Plant Methods* **14**, 34 (2018).

56. J. Yao, C. Allen, The plant pathogen *Ralstonia solanacearum* needs aerotaxis for normal biofilm formation and interactions with its tomato host. *J. Bacteriol.* **189**, 6415–6424 (2007).
57. S. Ouyang, G. Park, H. S. Atamian, C. S. Han, J. E. Stajich, I. Kaloshian, K. A. Borkovich, MicroRNAs suppress NB domain genes in tomato that confer resistance to *Fusarium oxysporum*. *PLOS Pathog.* **10**, e1004464 (2014).
58. N. Schandry, A practical guide to visualization and statistical analysis of *R. solanacearum* infection data using R. *Front. Plant Sci.* **8**, 623 (2017).

Acknowledgments: We thank S. Ouyang from Yangzhou University for sharing the *Fol* strain and Y. Liu from Huazhong Agricultural University for the help with EPS extraction. We appreciate J. Li from Sun Yat-sen University and G. Wang from Fujian Agriculture and Forestry University for the suggestions on our research. **Funding:** The study was supported by the National Natural Science Foundation of China (grant no. 32272556 to B.L.), Hubei Special Project for Science Development (2024CSA060 to B.L.), Fundamental Research Funds for the Central Universities (grant no. 2662023PY006 to B.L.), and Funds of the National Key Laboratory of Agricultural Microbiology (grant no. AML2023C01 to B.L.). **Author contributions:** Conceptualization: D.J. and B.L. Methodology: W.Z., S.C., J.K., and J.X. Validation: W.Z., S.C., M.H., J.K., J.X., D.J., and Y.F. Formal analysis: W.Z., S.C., J.K., J.X., X.Y., and B.L. Investigation: W.Z., S.C., M.H., P.L., J.K., A.X., and D.J. Resources: P.L., J.K., Y.L., J.C., D.J., and B.L. Data curation: Y.L. and X.Y. Writing—original draft: W.Z., S.C., X.Y., and B.L. Writing—review and editing: J.X., J.C., Y.F., X.Y., and B.L. Visualization: W.Z., S.C., J.C., and B.L. Supervision: Y.L., J.X., D.J., and B.L. Project administration: J.C., D.J., and B.L. Funding acquisition: B.L. **Competing interests:** The authors declare that they have no competing interests. **Data and materials availability:** All data needed to evaluate the conclusions in the paper are present in the paper and/or the Supplementary Materials. All the original MS data had been uploaded to ProteomeXchange (PRIDE) Consortium via the iProX partner repository with the dataset identifier PXD055434. The plasmids, transgenic plants, and unique reagents generated in this study are available from the lead contact B.L. (boli@mail.hzau.edu.cn) with a completed Material Transfer Agreement.

Submitted 31 October 2024
Accepted 24 April 2025
Published 30 May 2025
10.1126/sciadv.adu2840